

Academic Year 2019-2020

Faculty Pharmaceutical, Biomedical and Veterinary
Sciences

Biomedical Sciences



Gene insertion and excision: a step towards the reversible immortalisation of human corneal endothelial cells

By:

Wout Arras

Master Thesis in partial fulfillment of the requirements for the degree

Master in Biomedical Sciences

Promotor: Prof. dr. Carina Koppen

Copromotor: dr. Bert Van den Bogerd

ARGOS – Antwerp Research Group for Ocular Science
Campus Drie Eiken, T-building
Universiteitsplein 1
2610 Wilrijk
Belgium

Acknowledgements

This master's thesis and accompanying internship are an objective for graduating Biomedical Sciences and were conducted at the Antwerp Research Group for Ocular Science (ARGOS). During my internship, I received help from several people whom I would like to thank.

Foremost, I would like to express my gratitude to my cosupervisor dr. Bert Van den Bogerd for mentoring me during all aspects of this master's thesis from my writings to presentations, and dr. Steffi Matthyssen for her feedback, support and understanding. I sincerely thank Prof. dr. Carina Koppen for supervising this project and her kindness throughout this period. They gave me the opportunity to present my project at the Dutch Ophthalmology PhD Students' conference meeting and apply for an FWO fellowship. I am also grateful to Hendrik Vercaammen and Sara Van Acker for their help and friendship.

They all made me feel welcome at ARGOS and caused my internship to be a valuable addition to my study.

Lastly, I would be remiss not to thank Myrthe Geelen for her mental support and keen eye in detecting formatting flaws.

I wish all of them the best for the future,

Wout

Abstract

The corneal endothelium is the most posterior layer of the human cornea. Its main function comprises the removal of excessive water from the cornea in order to sustain its state of deturgescence. Accelerated loss of human corneal endothelial cells (HCEncs) can cause the cornea to swell which leads to a reduction of visual acuity and eventually blindness. Corneal transplantation is the only therapy that can offer a definitive cure. Unfortunately, the low donor to patient ratio causes 12.7 million people to await corneal transplantation worldwide, of which a major part is due to corneal decompensation. The endothelial donor shortage also affects research as it now depends on the limited amount of endothelia that are rendered unsuitable for transplantation and immortalised cell lines.

To aid in the development of ex vivo engineered corneal endothelia and provide a better alternative for immortalised cell lines, the reversible immortalisation of HCEncs is proposed. In this master's thesis, different experiments were performed to evaluate its most elemental aspects related to the construct integration and puromycin selection. The objectives comprised: (I) finding the multiplicity of infection (MOI) and exposure time needed to obtain a transduced cell yield of 20-30%, (II) compare the integration efficiency between a viral (lentiviral) and non-viral (PiggyBac) vector, (III) determine the strongest promoter to drive future oncogene transcription and (IV) decide what puromycin concentration and exposure time is needed to eradicate non-puromycin resistant cells.

To allow for an easy quantifiable readout of the different aspects of construct integration, the enhanced green fluorescent protein gene (*eGFP*) was used. The optimal MOI (range 0-30) and exposure time (4- or 24-hours) to obtain a transduced cell yield of 20-30% was determined by using live cell imaging and flow cytometry. The latter was also used to compare the strength of four *eGFP* driving promoters (CypA, CBA, EF1a and SFFV) by measuring the intensity of *eGFP* expression after lentiviral integration. To assess potentially harmful effects of transduction, the population doubling time was calculated at different MOIs and after 4- and 24-hours of viral exposure. Since the PiggyBac vector cannot autonomously enter the cell, its introduction was mediated through lipofection. In order to select puromycin-resistant cells in the future, the dose (range 0-10 µg/mL) and exposure time (0-, 24-, 48-, or 72-hours) of puromycin needed to eradicate unmodified cells was determined by using live cell imaging and a luminescence microplate reader. All these experiments were conducted in an immortalised cell line (HCEC-B4G12).

The quantification of *eGFP* positive cells after viral transduction indicated that the percentage of transduced cells was directly proportional to the MOI. Also an increase of exposure time from 4- to 24-hours resulted in a higher *eGFP* positive cell yield. Under the experimental conditions described in this project, lentiviral transduction was found to be very efficient. However, no *eGFP* expressing cells could be detected after transfection with the PiggyBac vector. From the four promoters that were compared, the mean *eGFP* intensity was the highest in the construct containing the SFFV promoter. Overall, the viral transduction did not cause an increase in population doubling time except when exposed for 24-hours to a relatively high MOI (≥ 30).

Depending on the construct and time of viral exposure, the desired transduction efficiency of 20-30% was obtained by using an MOI between 0.3 and 1. For the strongest promoter (SFFV), this transduced cell yield was obtained after 24-hours of viral exposure to MOI 0.5. In contrast, transfection with the PiggyBac vector did not result in any detectable *eGFP* positive cells which most likely indicates a low transfection efficiency or an incompatibility between the used cell line and the transfection reagent. To isolate puromycin-resistant cells in the future, the cells can be exposed for 72-hours to 2 µg/mL puromycin since this was found to be lethal for all non-resistant B4G12 cells.

Samenvatting

Het corneale endotheel is de binnenste laag van de cornea. Deze laag staat in voor het wegpompen van het overmatige water uit de cornea waardoor deze in een optimaal gehydrateerde staat wordt gehouden en zo zijn doorzichtigheid garandeert. Een versnelt verlies van humane corneale endotheelcellen (HCEC) kan er voor zorgen dat de cornea begint te zwellen. Hierdoor verminderd het gezichtsvermogen en kan de patiënt op lange termijn zelfs blind worden. De enige oplossing is een corneatransplantatie, maar door de grote nood aan donorweefsel zijn er wereldwijd 12,7 miljoen mensen die wachten op een donor cornea waarvan meer dan de helft een gevolg is van corneale decompensatie. Ook het wetenschappelijk onderzoek lijdt onder dit donortekort aangezien de huidige experimenten voornamelijk uitgevoerd worden met geïmmortaliseerde cellijnen of donor weefsel dat niet geschikt is voor transplantatie.

In deze master thesis wordt de reversibele immortalisatie van HCEC voorgesteld als beter alternatief voor geïmmortaliseerde cellijnen en voor de ontwikkeling van kunstmatige endotheliale weefsels. Het doel was om de elementaire aspecten van reversibele immortalisatie te verhelderen met de nadruk op construct integratie en puromycine selectie. Hiervoor werden volgende tussendoelstellingen vastgelegd: (I) het vinden van de concentratie aan virale vectoren en blootstellingstijd die nodig zijn om 20-30% getransduceerde cellen te bekomen, (II) een vergelijking maken tussen de integratie efficiëntie van een virale (lentiviraal) en niet-virale (PiggyBac) vector, (III) bepalen wat de sterkste promotor is om een oncogen aan te drijven in de toekomst en (IV) beslissen welke concentratie en blootstellingstijd aan puromycine letaal is voor alle niet-puromycine resistente cellen.

Om de verschillende aspecten van de construct integratie te kwantificeren wordt gebruik gemaakt van het enhanced green fluorescent protein gen (*eGFP*). De optimale virale concentratie (MOI 0-30) en blootstellingstijd (4 of 24 uur) om 20-30% getransduceerde cellen te bekomen werd bepaald aan de hand van live cell imaging en flowcytometrie. Deze laatste werd ook gebruikt om de sterkte van vier promotoren (CypA, CBA, EF1a en SFFV) te vergelijken op basis van *eGFP* expressie intensiteit. Als maatstaf voor een potentieel toxisch effect van transductie, werd de populatie dubbelingstijd berekend. In tegenstelling tot de gebruikte virussen, kan de PiggyBac vector niet autonoom in de cel geraken. De introductie van de PiggyBac vector werd daarom gemedieerd door middel van lipofectie. De letale puromycine concentratie (0-10 $\mu\text{g}/\text{mL}$) en blootstellingstijd (0, 24, 48 en 72 uur) werden bepaald door de hoeveelheid levende cellen te kwantificeren d.m.v. live cell imaging en fotospectrometrie. Alle experimenten in dit project waren uitgevoerd op een geïmmortaliseerde cellijn (HCEC-B4G12).

De kwantificatie van het aantal *eGFP* positieve cellen na transductie toonde een recht evenredig verband aan tussen het percentage getransduceerde cellen en de virale concentratie. Ook een verhoging van de blootstelling van 4 naar 24 uur resulteerde in een groter aantal *eGFP* positieve cellen. Van de vier geëvalueerde promotoren, leidde SFFV tot de hoogste gemiddelde *eGFP* intensiteit. In tegenstelling tot lentivirale transductie, werden geen *eGFP* positieve cellen gedetecteerd na transfectie van de PiggyBac vector. Daarnaast werd vastgesteld dat transductie enkel resulteert in een verhoogde populatie dubbelingstijd bij 24 uur blootstelling aan een relatief hoge virale concentratie (\geq MOI 30).

Afhankelijk van het construct en virale blootstellingstijd, kan de gewenste transductie efficiëntie van 20-30% bereikt worden met behulp van een virale concentratie tussen MOI 0,3 en 1. Voor de sterkste promotor (SFFV), werd de gewenste transductie efficiëntie bereikt na 24 uur blootstelling aan MOI 0,5. Het gebrek aan *eGFP* expressie na transfectie van de PiggyBac vector is waarschijnlijk het gevolg van een lage transfectie efficiëntie ten gevolge van een incompatibiliteit tussen de gebruikte cellijn en het transfectie reagens. Voor de isolatie van puromycine-resistente cellen in de toekomst, kunnen de cellen blootgesteld worden gedurende 72 uur aan een concentratie van 2 $\mu\text{g}/\text{mL}$ aangezien dit letaal werd bevonden voor alle niet-resistente B4G12 cellen.

As a result of the COVID-19 pandemic, the experiments for this project were discontinued for an undetermined period. However, its impact on this master's thesis is only moderate as a major part of the experiments was already executed. From the four work packages that comprised the original project (Fig. A1), three parts were almost finished. The remaining time was spent by doing a thorough analysis of the obtained results and an additional assignment was given. This assignment comprised the writing of the main parts of a review about a subject of choice related to the corneal endothelium.

Table of content

Acknowledgements	2
Abstract	3
Samenvatting.....	4
List of abbreviations	8
1 State of the art.....	9
1.1 Basic characteristics of the human cornea.....	9
1.1.1 Epithelium	9
1.1.2 Bowman’s layer	9
1.1.3 Stroma	9
1.1.4 Descemet membrane	10
1.1.5 Endothelium	10
1.2 A detailed view on the human corneal endothelium.....	10
1.2.1 (Lack of) endothelial cell proliferation	10
1.2.2 Pathologies of the corneal endothelium	11
1.3 Reversible immortalisation	13
1.3.1 Cell immortalisation by viral oncogene introduction.....	13
1.3.2 Lentiviral vectors	13
1.3.3 DNA transposon systems.....	14
1.4 Suicide gene-based selection mechanisms	15
1.4.1 Gene-directed enzyme prodrug therapy.....	15
1.4.2 Dimerisation inducing suicide mechanisms	15
1.4.3 Therapeutic monoclonal antibody-mediated suicide mechanisms	16
2 Research hypothesis.....	17
3 Materials and methods.....	18
3.1 Cell culture.....	18
3.2 Construct integration assays	18
3.2.1 Vectors.....	18
3.2.2 Multiplicity of infection	18
3.2.3 Assessment of eGFP expression	19
3.3 Puromycin selection	19
3.4 Statistical analysis.....	19
4 Results.....	20
4.1 Live cell imaging analysis.....	20

4.2	Construct integration	21
4.2.1	Kinetics of eGFP expression after transduction	21
4.2.2	Viral transduction efficiency.....	21
4.2.3	eGFP expression intensity	23
4.2.4	Toxicity of transduction.....	24
4.2.5	PiggyBac transfection efficiency.....	25
4.3	Puromycin kill curve	26
4.3.1	Live cell imaging.....	26
4.3.2	Luminescence microplate reader	27
5	Discussion	28
5.1	Construct integration	28
5.1.1	Influence of multiplicity of infection, promoter and exposure time on transduction efficiency.....	28
5.1.2	Comparative analysis between live cell imaging analysis and flow cytometry to determine the percentage of eGFP positive cells.....	29
5.1.3	Relation between the observed transduction efficiency and literature	29
5.1.4	Determining the strongest promoter.....	30
5.1.5	Toxicity of viral transduction	30
5.1.6	Transfection of the PiggyBac vector.....	30
5.2	LD ₁₀₀ of puromycin in the B4G12 cell line	31
6	Conclusion and perspectives	32
	Bibliography.....	33
	Appendix.....	38

List of abbreviations

ADCC	Antibody-dependent cellular cytotoxicity
bp	Base pairs
CBA	Chimeric cytomegalovirus-chicken β -actin
CDC	Complement-dependent cytotoxicity
CDKs	Cyclin-dependent kinases
CID	Chemical inducer of dimerisation
CKIs	Cyclin-dependent kinase inhibitors
CypA	Cyclophilin A
DM	Descemet membrane
DMEK	Descemet membrane endothelial keratoplasty
DSAEK	Descemet stripping automated endothelial keratoplasty
ECD	Endothelial cell density
EF1a	Elongating factor-1a
eGFP	Enhanced green fluorescent protein
EnMT	Endothelial-to-mesenchymal transition
FECD	Fuchs' endothelial corneal dystrophy
fLuc	Firefly luciferase
GAGs	Glycosaminoglycans
GCV	Ganciclovir
GDEPT	Gene-directed enzyme prodrug therapy
HCEncs	Human corneal endothelial cells
HIV-1	Human immunodeficiency virus type 1
HSV-TK	Herpes simplex virus thymidine kinase
hTERT	Human telomerase reverse transcriptase
iCasp9	Inducible caspase 9
IHC	Immunohistochemical
ITR	Inverted terminal repeat
LD ₁₀₀	Lethal dose 100%
LTR	Long terminal repeat
mAb	Monoclonal antibody
MOI	Multiplicity of infection
PD	Population doublings
qPCR	Quantitative real-time PCR
RCL	Replication-competent lentivirus
RNAi	RNA interference
SFFV	Spleen focus-forming virus
SIN	Self-inactivating
UZA	Antwerp University Hospital
VSV-G	Vesicular stomatitis virus
ZO-1	Zonula occludens-1

1 State of the art

1.1 Basic characteristics of the human cornea

The human cornea is the transparent tissue covering the anterior part of the eye (Fig. 1A). It is responsible for two thirds of the eye's refractive power and provides protection for its inner structures [1]. Measuring about 11.5 mm horizontally and 10.5 mm vertically, the cornea is slightly oval [2]. The tissue is avascular and comprised out of five layers: an epithelium, Bowman's layer, stroma, Descemet membrane and an endothelium which have a combined thickness of roughly 560 μm centrally and 630 μm at the periphery (Fig. 1B) [2,3].

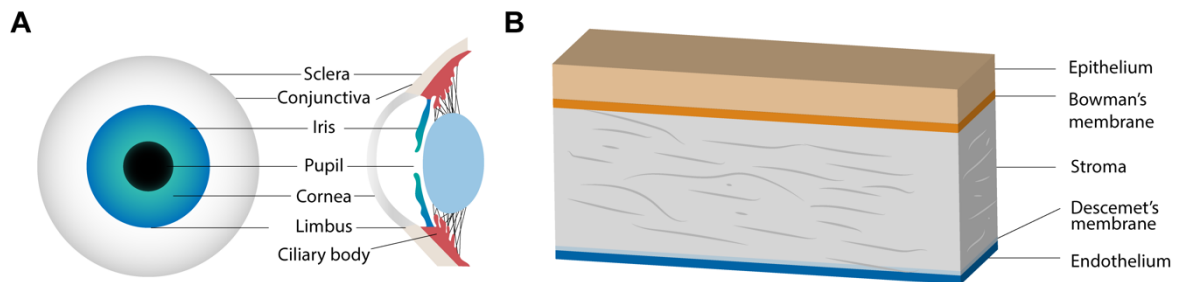


Figure 1: (A) Basic anatomy of the anterior human eye. (B) Overview of the five corneal layers.

1.1.1 Epithelium

The most superficial layer of the cornea is the epithelium. It has a thickness of 50 μm and is embryologically derived from the surface ectoderm. The corneal epithelium consists of four to six layers of non-keratinised stratified squamous epithelial cells. The most superficial cell layers have microvilli on their apical surface that are covered with a glycocalyx which functions as a lubricant and keeps the ocular surface hydrated [2,4]. The suprabasal cells, located in the lowest layers of the epithelium, are interconnected through tight junctions that prevent water and pathogens from leaking into the stroma [2]. Constant renewal of the corneal epithelium is achieved by the stem cells residing in a niche at the corneal-scleral transition, called the limbus (Fig. 1A) [5]. According to the XYZ hypothesis of Thoft and Friend published in 1983, the maintenance of the corneal epithelium can be depicted as three independent phenomena being: the proliferation of epithelial cells (X), the centripetal movement of basal epithelial cells (Y) and loss of epithelium on the corneal surface (Z). Therefore, corneal epithelial maintenance requires the sum of X and Y to be equal to Z [6].

1.1.2 Bowman's layer

The Bowman's layer is located at the basal side of the epithelium. This acellular layer is about 15 μm in thickness and composed out of randomly oriented collagen type I fibrils which are clearly distinguishable from the collagen fibrils of the stroma [7,8].

1.1.3 Stroma

The stroma accounts for 90% of the entire corneal thickness and is derived from neural crest cells. It is composed of heterodimeric fibrils of collagen types I and V which are organised in a parallel manner thereby forming different layers or lamellae [9,10]. The stroma consists of approximately 200 sheets of lamellae, each orthogonally oriented relative to its adjacent lamellae (Fig. 2) [11]. This specific arrangement confers strength to the cornea while the regular spacing between the fibrils, in combination with their uniform diameter, ensures stromal transparency. The most abundant cell type of the stroma are the keratocytes. These cells are crucial to maintain the stromal homeostasis by producing collagen, matrix metalloproteinases and glycosaminoglycans (GAGs) [1].

Due to their hydrophilic character, the repulsing GAGs give the stroma the tendency to attract water and nutrients from the anterior chamber while also regulating the spacing between the collagen fibrils [12]. However, if the stroma gets too hydrated, disturbances of its intrinsic architecture will increase light scatter causing visual impairment [1].

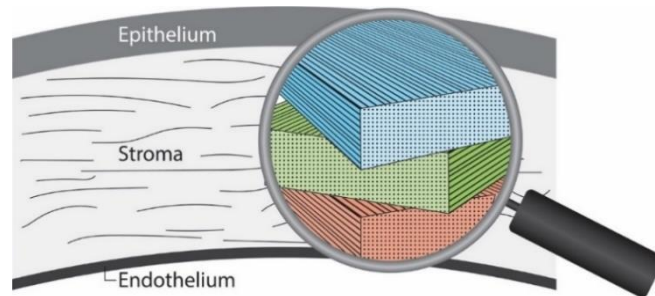


Figure 2: Specific arrangement of the stromal lamellae.

1.1.4 Descemet membrane

The stromal and endothelial layer of the human cornea are separated by an acellular layer called the Descemet membrane (DM). The development of DM can be divided in a prenatal and postnatal phase. In the prenatal phase, the endothelial cells secrete membrane components in a sequential manner establishing the anterior banded layer. This layer is composed of both type IV and VIII collagen. After birth, the endothelial cells produce the posterior non-banded layer by secreting non-striated homogeneous material containing only collagen type IV [13].

1.1.5 Endothelium

The most posterior layer of the cornea consists of a uniform monolayer of endothelial cells, which similarly to the stroma, originates from the neural crest [14]. Human corneal endothelial cells (HCEncs) have a thickness of about 5 μm and a diameter of 20 μm . They span the entire posterior cornea until they merge with the cells of the trabecular meshwork at the periphery [15].

The HCEncs are interconnected through focal tight junctions located at the apical part of their lateral membranes. Towards the basal side of these membranes, sinuous interdigitations can be found which are connected by a combination of gap and adhesion junctions [14]. These junctions cause the endothelium to function as a leaky barrier. This allows the diffusion of nutrients into the cornea, while its waste products can be recycled to the anterior chamber [14,16]. To assist the exchange of nutrients and waste products, the HCEncs contain carriers for facilitated diffusion (Glut1) and secondary active transport (lactate/ H^+ and lactate/ Na^+). In addition to the diffusion of molecules, the endothelium allows the stromal imbibition pressure generated by the hydrophilic GAGs to attract water from the anterior chamber [16]. But in order for the stroma to maintain its state of relative dehydration (i.e. stromal deturgescence), the HCEncs also function as a pump by removing the excess of water. While it is clear that multiple ion transporter mechanisms on the HCEncs (e.g. anion channels and Na^+/K^+ -ATPase) play an important role, the exact mechanism behind the corneal endothelial pump function remains controversial [12].

1.2 A detailed view on the human corneal endothelium

1.2.1 (Lack of) endothelial cell proliferation

In the first year after birth, the endothelial cell density (ECD) is about 4000 cells/ mm^2 but decreases rapidly due to corneal growth until the age of two. Age-related apoptosis causes the ECD to decrease further at a steadier attrition rate of 0.3-0.6% each year throughout life [17–19]. Whether HCEncs are able to proliferate in vivo remains a matter of debate, but it is clear that HCEncs lack sufficient proliferative capacity to compensate for their loss [20].

Therefore, the endothelial cells migrate and enlarge in response to the continuously decreasing ECD, causing the cells to change from a hexagonal to a pleomorphic shape over time. These compensation mechanisms allow the corneal endothelium to maintain its function, although with an overall reduced pumping capacity [14,18].

Based on the expression and localisation of cyclins (i.e. cell cycle dependent proteins) it was found that HCEncs are arrested in the early G1 phase of the cell cycle [21]. This cell cycle arrest is thought to be caused by a combination of three mechanisms being: endothelial cell-cell contact inhibition, inadequate amounts/binding of growth factors and the inhibition of S-phase entry by TGF β 2 [22]. Notwithstanding these cells lack proliferative capacity *in vivo*, *ex vivo* studies showed that replication of HCEncs can be induced by the expression of viral oncoproteins (i.e. SV40 large T antigen or E6/E7) or transcription factors (i.e. E2F2) [23–25]. This indicates that HCEncs at least possess the potential to proliferate [14].

Due to the relatively large number of HCEncs at birth and their slow rate of apoptosis, the lack of corneal endothelial proliferation usually does not cause a decrease of corneal transparency. However, the loss of HCEncs can be accelerated as a result of trauma, refractive surgery, cellular stress caused by diabetes or glaucoma, but also due to certain corneal endothelial pathologies. In general, a cell density of 400-500 cells/mm² is considered to be the threshold from which point the endothelial pump capacity is not able to counteract the water leaking into the stroma causing visual acuity to get affected [15,22].

1.2.2 Pathologies of the corneal endothelium

1.2.2.1 Fuchs' endothelial corneal dystrophy

Different primary corneal endothelial pathologies exist which eventually lead to endothelial cell dysfunction, the most common being Fuchs' endothelial corneal dystrophy (FECD) [26,27]. This endothelial pathology is currently the primary indication for corneal transplantation worldwide [27].

FECD is an inherited bilateral disease characterised by the accelerated loss of endothelial cells which is accompanied by their enlargement and loss of hexagonal shape. Also an aberrant deposition of extracellular matrix and the formation of DM projections, termed guttae¹, in between HCEncs are important hallmarks of this disease (Fig. 3A) [28]. FECD slowly progresses over the course of 20-30 years in which the patient goes through four stages [26]. At first, non-confluent guttae will appear in the centre of the cornea. These guttae force the surrounding endothelial cells to adopt a rosette-like clustering (Fig. 3B) and progressively induces apoptosis in these cells. In this stage, the endothelial compensation mechanism is able to safeguard the patient from any symptoms. As disease progresses to the second stage, the guttae start to coalesce and also appear in the periphery. The increase in guttae goes hand in hand with a decrease in ECD which diminishes the "pump-and-leak" function of the corneal endothelium. The stromal deturgescence will become compromised and the resulting corneal oedema causes the patient to experience blurred vision. In the third stage, stromal oedema progresses towards the epithelium causing bullous keratopathy to arise (i.e. the formation of blisters under and between the corneal epithelial cells) [29]. This further reduces visual acuity and results in excruciating pain since the cornea is one of the most densely innervated human tissues [9,29]. In the final stage, the patient suffers from chronic bullous keratopathy which is characterised by corneal neovascularisation and stromal scarring causing the patient to turn blind [26]. However, such advanced stage of FECD is uncommon in developed countries since patients are treated earlier in the disease process.

¹ Gutta (plural: Guttae) is the Latin word for "drop", originating from their resemblance to dewdrops when observed through a slit-lamp microscope [90].

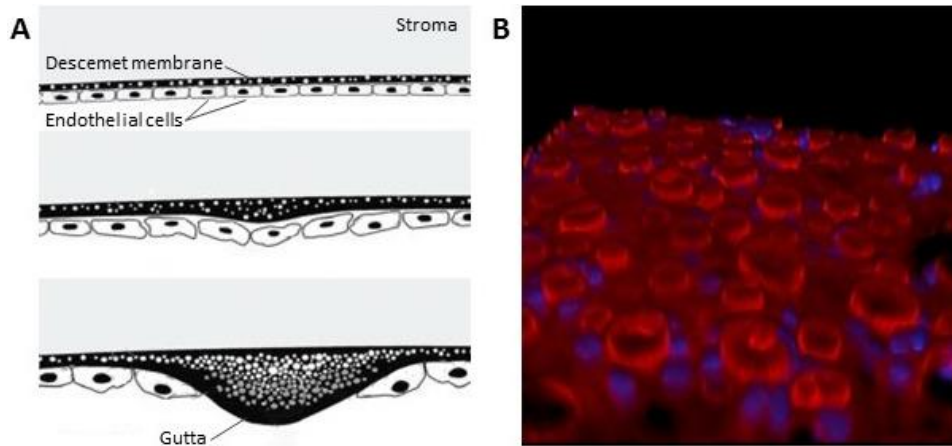


Figure 3: (A) Schematic representation of the gutta formation and the resulting pleomorphism and polymegathism of the HCEncs to compensate for the decrease in ECD [30]. (B) 3D representation of an ex vivo whole mount corneal endothelium of a Fuchs' corneal endothelial dystrophy patient stained for laminin (red) indicating the extracellular matrix and guttae (mushroom-shaped extrusions), and DAPI (blue) indicating the corneal endothelial cell nuclei (40x magnification) [20]. HCEncs, human corneal endothelial cells; ECD, endothelial cell density

1.2.2.2 Current treatment options

The only definitive treatment for endothelial decompensation is corneal transplantation [26]. Previously, the golden standard worldwide was the transplantation of a full cornea by using a full corneal thickness graft (i.e. penetrating keratoplasty). However, nowadays, selective endothelial transplantation, also called endothelial keratoplasty, is preferred because of the less invasive procedure and decreased risk of rejection [27]. Endothelial keratoplasty can be divided in Descemet stripping automated endothelial keratoplasty (DSAEK) and Descemet membrane endothelial keratoplasty (DMEK). In DSAEK the graft is composed of a small amount of posterior stroma together with DM and the corneal endothelium (Fig. 4A) while a DMEK graft only consists out of DM and the corneal endothelium (Fig. 4B). Both have their advantages and disadvantages, but when transplanted successfully, they allow faster recovery and better visual outcome compared to penetrating keratoplasty [20]. Unfortunately, the amount of patients in need of corneal transplantation outnumbers the amount of available grafts by 70:1, leaving about 12.7 million people awaiting transplantation [27].

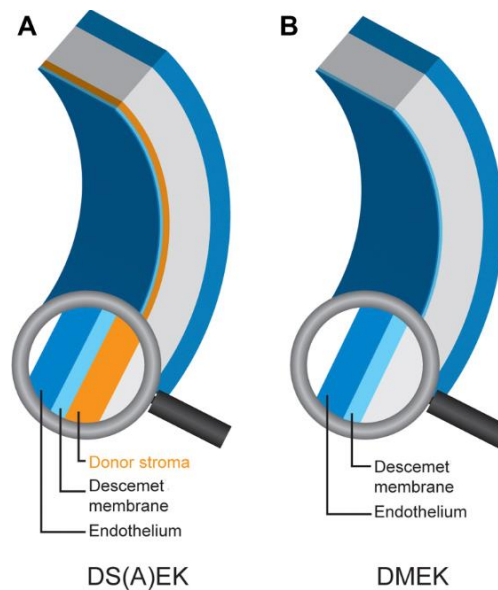


Figure 4: Simplified representation of the endothelial keratoplasty grafts. (A) In DS(A)EK, the donor graft consists of the endothelium, Descemet membrane and posterior stroma. (B) A DMEK graft only contains the endothelium and Descemet membrane. DS(A)EK, Descemet stripping (automated) endothelial keratoplasty; DMEK, Descemet membrane endothelial keratoplasty [20].

1.3 Reversible immortalisation

1.3.1 Cell immortalisation by viral oncogene introduction

Ex vivo expansion of HCEncs is thought of as an attractive tool to address the corneal donor shortage by aiding in the development of a corneal endothelium grown in the laboratory. This expansion can be accomplished by establishing the expression of viral oncogenes and/or human telomerase reverse transcriptase (*hTERT*) in the target cells to increase their proliferative capacity. Viral oncogenes generally function by inhibiting the p53 and p16/pRB pathways which are important for the cell cycle regulation [31]. However, the overexpression of an oncogene does not necessarily lead to fully immortalised cells. It is more likely that they will only increase the proliferative capacity of these cells until they enter a nondividing state due to a critically low telomere length (i.e. replicative senescence) [31,32]. Indeed, studies in which HCEncs are transduced with SV40 large T antigen reported a limited population doubling due to the occurrence of senescence [24,25].

To establish a fully immortalised cell line, replicative senescence needs to be avoided by increasing the telomerase function in the cells. Therefore, it can be opted to combine the introduction of *hTERT* with an oncogene [31,33]. This combination also has the advantage of decreasing the chance on chromosomal abnormalities compared to the transduction of an oncogene alone [31]. Depending on the phenotypical changes induced by immortalisation, removal of these genes by certain excision mechanisms (see further) could restore the cell to its original state [34].

1.3.2 Lentiviral vectors

Viral vectors are a popular tool for gene transduction due to their high transduction efficiency [35]. They account for roughly 70% of the vectors used in gene therapy clinical trials [36]. However, multiple types of viral vectors including adenoviral, retroviral, adeno-associated and lentiviral vectors are currently being used, each having their own characteristics (Appendix Table A1) [35]. Lentiviral vectors have the ability to stably transduce both dividing and non-dividing cells and contain a relatively large cargo capacity (± 9 kb) [37]. Therefore, they are good candidate vectors for the stable introduction of proliferation increasing genes in HCEncs.

Lentiviruses are members of the *Retroviridae* viral family. Different species of lentiviruses exist, but the human immunodeficiency virus type 1 (HIV-1) is the predominantly used lentiviral vector. Especially for clinical applications, safety measures are needed to prevent the generation of replication-competent lentiviruses (RCLs). RCLs arise due to recombination events (during production or in vivo) resulting in a vector that is able to express viral proteins. These proteins can cause replication of the recombinant lentiviruses comparable to that of wild-type viruses [37]. By separating the viral genes needed for viral vector production in different plasmids and removing non-essential viral proteins, the chance on RCLs during production is decreased. To date, four different generations of lentiviral vectors were developed, each generation having a superior safety profile compared to the previous [38–40]. These alterations in viral vector production were very effective considering that both in second and third generation HIV-1 vectors no RCLs have been observed [37]. Other safety measures include the use of self-inactivating (SIN) vectors. Here, deletion of the 3' long terminal repeat (LTR) causes the viral enhancer and promoter region to be lost upon integration [41]. Therefore, the inserted viral vector cannot be mobilised by a wild-type virus and the LTRs can no longer cause unintended overexpression or interference of nearby genes [37]. These safety measures cannot prevent the lentiviral vectors from causing gene disruption or overexpression due to the integration of the vector (i.e. insertional mutagenesis). However, such problems can be solved by excising the construct when it is no longer needed [37,42].

1.3.2.1 Cre-lox site-specific excision

To further increase the safety of integrated viral vectors, the Cre-lox system can be used to remove the vector when gene expression is no longer needed. This system consists of the Cre-recombinase enzyme and two loxP sites. Each loxP site is composed of two inverted repeats of 13 bp, separated by an 8 bp spacer which defines the orientation of the loxP site. The Cre-recombinase enzyme cuts in the spacer region creating 6 bp overhangs [43]. When a construct is flanked by two loxP sites (i.e. "floxed") in the same orientation, the Cre-recombinase excises the construct. The loxP overhangs will ligate causing circularisation of the construct and closure of the gap in the genome thereby leaving behind a footprint of one loxP site (Fig. 5). Alternatively, if the construct is flanked by inverted loxP sites, inversion of the construct can be achieved and if two separate strands contain a loxP site in the same orientation, intermolecular recombination (i.e. translocation) can occur [44].

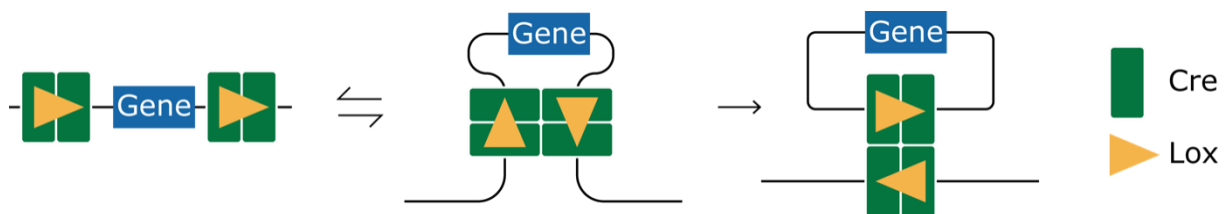


Figure 5: Excision of a gene flanked by two loxP sites with the same orientation [45].

1.3.3 DNA transposon systems

Transposons are DNA segments with the ability to move and/or replicate within the genome but are unable to propagate to other cells. DNA transposons employ a cut-and-paste mechanism which is utilised for their use as a non-viral vector [46]. In this regard, especially the PiggyBac system is a promising tool because it allows both integration and footprint-free removal of the construct [47].

The PiggyBac transposon, originally isolated from the cabbage looper moth (*Trichoplusia ni*), consists out of a transposase flanked by inverted terminal repeats (ITRs). Upon expression, the transposase recognises these specific ITRs and mobilises the transposon to insert it in another place of the genome [48]. This principle is adopted in genetic engineering, where the construct is flanked with ITRs and inserted in the genome by expression of PiggyBac transposase [49]. Further improvements have led to the development of an excision-competent, but integration-defective PiggyBac transposase, allowing to excise the construct without the risk of reintegration [50].

In contrast to viral vectors, PiggyBac vectors need additional techniques to allow their efficient introduction into the cell, such as electroporation or lipofection [49]. The cargo capacity of PiggyBac vectors can go up to 9 kb without a significant decrease in transposition efficiency [51]. Nevertheless, constructs up to 100 kb have been transposed using this system [52]. Integration of PiggyBac occurs almost exclusively (98%) at TTA sites in the genome and seems to have a preference towards promoters and active genes [53]. Compared to HIV-derived vectors, PiggyBac vectors are considered to have a safer integration profile because they are more likely to integrate in so-called "genomic safe harbours" (i.e. regions in the human genome where newly integrated DNA is not likely to cause adverse effects) which decreases the possibility of causing insertional mutagenesis [54].

1.4 Suicide gene-based selection mechanisms

Previously, it was discussed how the construct can be removed from genetically modified cells. Independent of the used technique, this removal is unfortunately not 100% efficient [50,55]. The remaining construct-containing cells could pose safety issues for human transplantation or make them less representative for primary cells when used in fundamental research. Therefore, all residual construct-containing cells need to be eradicated which can be done through the use of so-called "suicide genes".

Suicide genes encode certain proteins with the potential to cause selective destruction of the cells containing this gene [56]. The system can be applied in many fields such as gene therapy for cancer treatment, fail-safe in adoptive cell therapies but also as a selection mechanism in regenerative medicine [57,58]. In case of the latter, the ideal suicide gene is one that guarantees the eradication of exclusively these cells containing the construct. However, since the efficiency of a suicide gene depends on many factors, it is recommended to use a combination of two suicide genes. Based upon their mechanism of action, three groups of suicide gene technology can be distinguished:

- gene-directed enzyme prodrug therapy (GDEPT);
- dimerisation inducing suicide genes; and
- therapeutic monoclonal antibody (mAb) -mediated suicide genes [56].

1.4.1 Gene-directed enzyme prodrug therapy

The principle of GDEPT is based on inducing the expression of a non-endogenous enzyme (or an endogenous enzyme with a very low expression level) that converts a harmless prodrug into a toxic drug [59]. The best studied enzyme/prodrug pairs are herpes simplex virus thymidine kinase (HSV-TK)/ganciclovir (GCV), *Escherichia coli* cytosine deaminase/5-fluorocytosine, cytochrome P450/cyclophosphamide or ifosfamide and nitroreductase/CB1954 [60]. The difference between these GDEPT systems resides in the way they cause apoptosis and whether they are able to eradicate dividing and/or non-dividing cells. Since the activated prodrug of GDEPTs has often a small molecular weight, it can easily diffuse to other cells resulting in a bystander effect. As a result, the suicide gene-containing cell will also cause the neighbouring (non-suicide gene-containing) cells to die. This may seem useful when applied in cancer therapy, but it could potentially limit their use as a selection mechanism in regenerative medicine [61]. Nevertheless, Fang et al. successfully used the HSV-TK/GCV pair to eradicate all construct containing cells that were left after construct excision with the Cre-lox technique [55]. This indicates the potential of the HSV-TK system. The same enzyme/prodrug pair has also been used in a T-cell therapy called Zalmoxis. Here, allogeneic T cells were transduced with a construct containing the HSV-TK gene as a safety measure in case the patient would develop graft-versus-host disease [62]. This therapy was conditionally approved in 2016, but subsequently withdrawn from the market by its manufacturer in 2019 due to commercial reasons [63,64].

1.4.2 Dimerisation inducing suicide mechanisms

Dimerisation inducing suicide genes encode chimeric proteins consisting of a chemical inducer of dimerisation (CID)-binding domain linked with an endogenous proapoptotic molecule. Upon addition of a CID, the chimeric proteins dimerise through their CID-binding domain which causes the linked proapoptotic molecules to initiate apoptosis [56,65]. The inducible caspase 9 (iCasp9) with AP1903 as CID, is an example of such suicide gene/CID pair that has successfully been used in several clinical trials. In these trials, it is mainly used to kill donor-T cells if graft-versus-host disease occurs [66]. In contrast to the GDEPTs, iCasp9 is more selective (i.e. no bystander effect) and therefore causes no collateral damage [67].

1.4.3 Therapeutic monoclonal antibody-mediated suicide mechanisms

Therapeutic mAb mediated suicide genes cause cells to express specific proteins on their surface to which mAb can bind [56]. In vivo, these mAb cause death of the cells carrying these membrane proteins via complement-dependent cytotoxicity (CDC) and antibody-dependent cellular cytotoxicity (ADCC). Therefore, the in vitro use of this system (e.g. as a selection mechanism in regenerative medicine), has the disadvantage that the complement system and immune effector cells are usually not present to invoke CDC or ADCC respectively. A major advantage is the fact that these specific membrane proteins can be used to isolate or identify the suicide gene-carrying cells. It was also found that the expression of these types of suicide genes in T-cells did not result in alterations of phenotype or growth characteristics. Examples of therapeutic mAb mediated suicide systems are the combination of CD20 with rituximab, truncated human EGFR polypeptide with cetuximab and RQR8 with rituximab. These pairs were all developed with the main focus on T-cell therapies [68–70]. Therefore, when employing this technique on other cells, it is important to validate that the added mAb does not have any affinity for membrane proteins other than these expressed by the suicide gene.

2 Research hypothesis

Previously, it was discussed that there is a discrepancy between the available donor corneas and patients in need [27]. The lack of good quality donor material also tremendously hampers corneal endothelial research which is forced to rely on immortalised cell lines and corneas that are excluded for transplantation due to donor age, low ECD or certain diseases. While immortalised cell lines produce sufficient amounts of cells, they may not be very representative for primary HCEncs. Conversely, good quality primary HCEncs are representative for native HCEncs but can be scarce to come by [71]. Increasing the amount of HCEncs by ex vivo culturing is being investigated, but they usually undergo but a few cell divisions before becoming senescent or acquiring a fibroblast-like phenotype (i.e. endothelial-to-mesenchymal transition), thereby skewing results [72]. Ex vivo expansion of HCEncs via reversible immortalisation might combine the advantages of both immortalised cell lines and primary cells. This strategy has the potential to provide sufficient and good quality HCEncs to address donor shortages for both transplantation and fundamental corneal endothelial research. In addition, these cells could be implanted in cornea-on-chips which are currently being developed at the ARGOS laboratory.

In this master's thesis it will be attempted to perform the first steps towards the reversible immortalisation of HCEncs. In order to do so, a cell line (HCEC-B4G12) will be used to:

- (I) find the multiplicity of infection (MOI) and exposure time needed for the desired transduced cell yield of 20-30% for lentiviral transduction;
- (II) compare the integration efficiency between a viral (lentiviral) and non-viral (PiggyBac) vector;
- (III) determine the best promoter for future oncogene transcription by transduction with different lentiviral vector constructs; and
- (IV) decide the minimal concentration and exposure time to puromycin that is needed to eradicate all non-construct containing cells.

Conclusions of experiments I, II and III will be based on differences in the expression of enhanced green fluorescent protein (eGFP) determined by flow cytometry and live cell imaging analysis. During the entire project, special attention will be paid to changes occurring in the HCEncs that could pose a potential safety risks or decrease cell functionality thereby limiting their use for future applications. The project is subdivided in two work packages: construct integration and puromycin selection. These work packages are part of a bigger project of which the main goal is to establish the reversible immortalisation of primary HCEncs (Fig. A1). The content of the work packages performed in this master's thesis will be discussed further below.

3 Materials and methods

3.1 Cell culture

All experiments were carried out using an immortalised cell line (HCEC-B4G12) (Appendix Table A2) between passages 10 and 16. To promote cell adherence, a coating containing fibronectin, collagen and albumin (FNC Coating Mix, Athena Enzyme Systems, Baltimore USA) was added to the plastic surface of culture flasks and wells before cell seeding. The cells were maintained in Human-Endothelial-SFM (ThermoFisher, Massachusetts, USA) containing 10 ng/ml FGF-2 (Sigma-Aldrich, Missouri, USA) and cultured in the incubator at 37°C and 5% CO₂. Quantification of the cell numbers that were needed for the experiments was done by trypan blue staining (ThermoFisher, Massachusetts, USA) after which the cells were transferred to a counting chamber and an automated cell counting (Corning, New York, USA) was performed.

3.2 Construct integration assays

3.2.1 Vectors

Second generation SIN lentiviral vectors with different promoters were bought from Leuven Viral Vector Core. Each promoter constitutively drives the expression of an *eGFP* gene and all second-generation lentiviral vectors were pseudotyped with the glycoprotein of the Vesicular stomatitis virus (VSV-G).

The lentiviral vectors had the following composition:

- LV_EF1a-eGFP-P2A-fLuc stock: 4.56×10^7 TU/ml size: 13,389 bp
- LV_SFFV-eGFP-P2A-fLuc stock: 4.60×10^8 TU/ml size: 12,587 bp
- LV_CypA-eGFP-P2A-fLuc stock: 1.75×10^8 TU/ml size: 12,637 bp
- LV_CBA-eGFP-P2A-fLuc stock: 3.16×10^8 TU/ml size: 12,874 bp

Based on the *eGFP* expression intensity, the strongest promoter was selected. In the future, this promoter will be combined in a vector with *eGFP* and a puromycin resistance gene.

Non-viral transfection of HCEncs was performed by using the PiggyBac Transposon Vector System (System Biosciences, California, USA) consisting of the PiggyBac vector (PB513B-1) and the Super PiggyBac Transposase vector (PB210PA-1) (Figs. A2 and A3). Their introduction in the cell was accomplished by lipofection, using the PureFection Transfection Reagent (System Biosciences, California, USA).

3.2.2 Multiplicity of infection

The MOI was optimized towards one copy number/cell by aiming at a transduced cell yield of 20-30% to increase the efficiency of construct excision later on. To determine the optimal MOI for each lentiviral vector, the cells were seeded in a 96-well plate (Corning, New York, USA) after which a serial dilution of viral stock solution was added. These dilutions were made in the medium previously described in 3.1. In addition, the difference between 4- and 24-hour exposure to the different MOIs was assessed but due to the low viral titre of the CypA and EF1a construct, the viral solution was passed on from the 4-hour exposure wells to the 24-hour wells. After exposure, the viral dilutions were replaced with NuLight Rapid Red reagent containing medium (Sartorius, Göttingen, Germany) to fluorescently stain the cell nuclei. Transfection with the PiggyBac vector was done according to the manufacturer's manual but combined with the NuLight Rapid Red reagent as well.

3.2.3 Assessment of eGFP expression

The amount of eGFP positive cells was assessed by two independent techniques: live cell imaging (IncuCyte; Sartorius, Göttingen, Germany) and flow cytometry (CytoFLEX; Beckman Coulter, Suarlée, Belgium). In flow cytometry, a cell suspension is directly injected into a stream of fluid and converted to a single flow of cells through hydrodynamic focussing. Individual cells pass a laser beam causing the light to be refracted in all directions allowing for both qualitative and quantitative analysis. The qualitative analysis comprises information about size, structural complexity and intensity of fluorescent markers [73]. In contrast to flow cytometry, data acquisition through live cell imaging is non-destructive. The cells are imaged at regular time intervals and quantitative data is obtained by employing the internal software (IncuCyte, Sartorius, Göttingen, Germany) (see 4.1 Live cell imaging analysis). To validate the acquisition of quantitative data by live cell imaging, it was compared to flow cytometry for the determination of the percentage of eGFP positive cells which was used as a measure for transfection/transduction efficiency. Before flow cytometric analysis, the triplicates were pooled and fixated with 1% paraformaldehyde to kill the remaining viruses. Apart from the percentage of eGFP positive cells, flow cytometry was also used to determine the eGFP expression intensity.

3.3 Puromycin selection

To isolate HCEncs containing a puromycin resistance gene in the future, a dose-response curve was made in order to find the minimal dose of puromycin (ThermoFisher, Massachusetts, USA) at which 100% of the non-puromycin resistant containing cells die within 2-3 days (LD₁₀₀). This will be the minimal concentration of puromycin needed for the selection of construct containing cells [74]. To determine the amount of viable cells, two methods have been used. The first method relies on live cell imaging combined with NuLight Rapid Red reagent staining. Secondly, the cells were exposed to PrestoBlue (ThermoFisher, Massachusetts, USA) for 30 minutes, after which the solution was transferred to a μ Clear plate (Greiner Bio-One, Kremsmünster, Austria). The metabolization of PrestoBlue was quantified by using a luminescence microplate reader (VICTOR, PerkinElmer, Massachusetts, USA) (emission filter set at 590 nm).

3.4 Statistical analysis

Because the replicates were pooled before performing a flow cytometric analysis and the experiments were only done once, statistical testing was done with the data derived from the live cell imaging analysis.

For statistical testing of the data obtained through live cell imaging, non-parametric testing was employed due to the low sample size. The following statistical tests were employed:

- The Kruskal Wallis test followed by a post-hoc Dunn's multiple comparison test was done to compare the different promoters based on transduction efficiency and population doubling time. It was also used to assess if the population doubling time significantly differed at certain MOIs for each promoter individually.
- Statistical testing of the percentage eGFP positive cells and population doubling time between 4- and 24-hours of viral exposure for each promoter, was done by using multiple t-tests.

Throughout all experiments, a $p < 0.05$ was considered to be indicative of a significant difference. Statistical analysis was conducted with Prism v8 software (GraphPad, California, USA) and the flow cytometric data was analysed using FlowJo v10.2 (TreeStar Inc, Oregon, USA).

4 Results

4.1 Live cell imaging analysis

In this project, live cell imaging was regularly employed because it allows for the assessment of various cell parameters in time, in a non-destructive manner. Such non-destructive methods enable the use of subsequent downstream assays with the same samples which reduces the interexperimental variability. Therefore, it would be the method of choice to determine the amount of eGFP positive cells and the total amount of cells in future experiments compared to destructive methods like flow cytometry. With live cell imaging, images were taken in a red, green and phase-contrast channel (Fig. 6A-C) at fixed time points around the clock. Objects can be quantified on the base of contrast or fluorescence with the help of the internal software. By finetuning some of the software's parameters, a mask (i.e. digital representation of the objects of interest) can be made for a set of images. For example, the amount of NuLight Rapid Red reagent stained nuclei (Fig. 6A) were detected by a mask as separate objects (Fig. 6D), which were then quantified as the amount of objects per mm^2 at each time point. Because each nucleus should be fluorescently stained, the amount of object per mm^2 gives an accurate assessment of cell count. However, some images contain artifacts like the bright red objects present in Figure 6A (white arrow). These do not represent living cells and were consistently excluded from the mask based on their high intensity (Fig. 6D white arrow). The accuracy of each mask was assessed and adapted for all experiments individually to exclude such artifacts.

In contrast to the fluorescently stained nuclei, the eGFP signal was quite diffuse (Fig. 6B) which made it difficult to accurately fit the mask for each individual cell (Fig. 6E). This causes the number of individual objects per mm^2 to be an underestimation of reality. Therefore, a third mask was made (Fig. 6F), in which each object (blue) represents a fluorescently stained nucleus overlapping with an eGFP positive signal. In this way, the amount of eGFP expressing cells were determined more accurately.

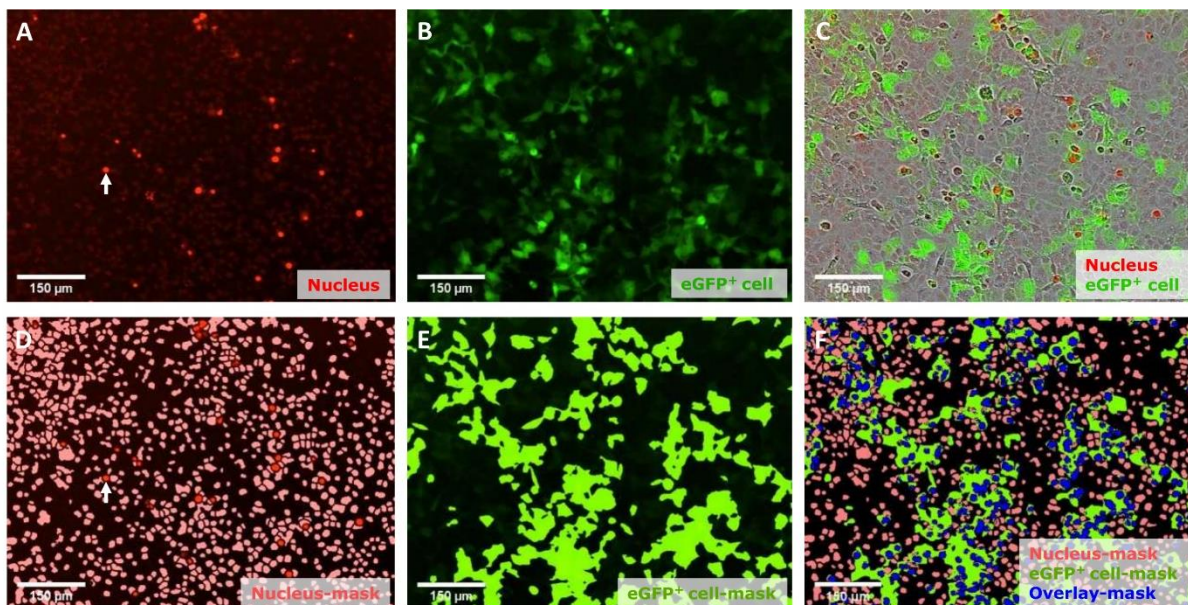


Figure 6: Images of MOI 5, 52 hours after transduction, from the 4-hour exposure experiment (SFFV promoter) and their accompanying masks that were used for data analysis. (A) In the red channel the cell nuclei are visible due to staining with NuLight Rapid Red reagent (white arrow indicates artefact), while the green channel (B) clearly indicates the presence of eGFP expressing cells. (C) Both the green and red channel are combined with the phase-contrast image giving a better perspective of the cell borders. D is a representation of the mask that was used to identify the cell nuclei (pink, white arrow indicates artefact that is not included in the mask) and E shows the mask for the eGFP expressing cells (bright green). The overlap between the masks represented in D and E was used to determine the amount of eGFP positive cells (F, blue). This overlay-mask provides a better quantifiable representation of the amount of eGFP positive cells because single objects can be better defined. eGFP, enhanced green fluorescent protein; SFFV, spleen focus-forming virus

4.2 Construct integration

4.2.1 Kinetics of eGFP expression after transduction

Live cell imaging was used to observe the progression of eGFP expression in the B4G12 cell line every 2 hours (Fig. 7). The presence of the viral vector-containing medium interfered with the detection of eGFP expression. This made it impossible to determine the amount of eGFP positive cells during the incubation with the virus for 4- and 24-hours. eGFP expression could be detected at 17 ± 3 hours after the initiation of transduction. In the 4-hour of viral exposure experiment, the eGFP expression kinetics indicated a sigmoid function that reached a plateau phase after ± 60 hours (see Fig. 7 and A4 A-H for other promoters).

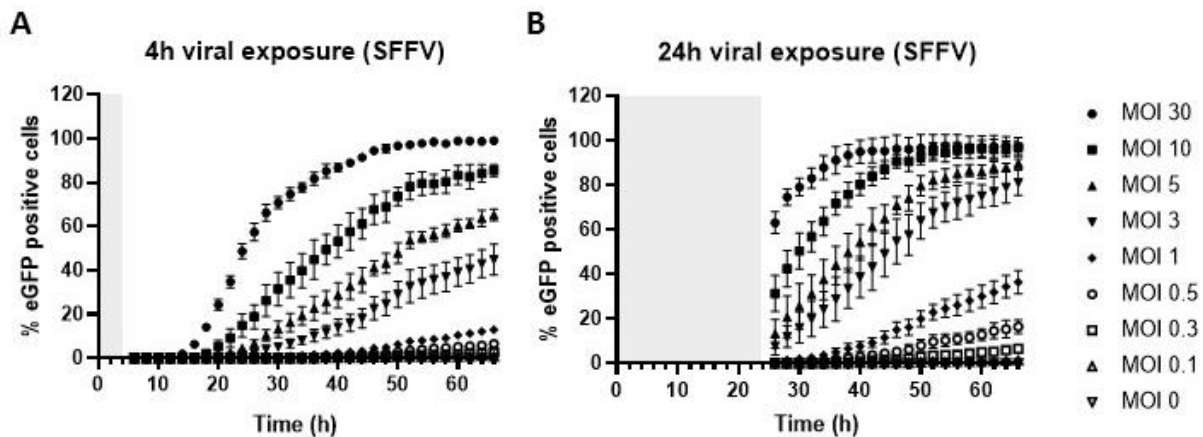


Figure 7: Example of eGFP expression kinetics after lentiviral transduction in the B4G12 cell line (SFFV promoter). The percentage of eGFP positive cells is represented as a function of time after removal of viral vectors from the 4- (A) and 24-hour (B) exposure experiment ($n=3$). The grey box represents the incubation time during which no measurements could be taken due to interference with the viral vector. eGFP, enhanced green fluorescent protein; SFFV, spleen focus-forming virus

4.2.2 Viral transduction efficiency

4.2.2.1 Live cell imaging

In order to obtain the target transduction efficiency of 20-30%, a B4G12 cell line was exposed to a range of MOIs between 0 and 30 which was repeated for each promoter construct individually. The cells were exposed to a certain MOI for 4- and 24-hours to assess the effect of viral exposure time on the transduction efficiency. The amount of eGFP positive cells was determined based on live cell imaging.

The results indicated that an increase in MOI also caused the percentage of eGFP positive cells to increase (Fig. 8). Statistical testing revealed that the transduction efficiency significantly differs between the different promoters. It was found that the experiments with the CypA promoter construct resulted in a significantly increased transduced cell yield at some of the MOIs compared to other promoters. However, it must be noted that these significant differences also occur between controls and in the lower MOI range which means these differences are probably caused by promoter-independent variations between the experiments. An overview of the different p-values for the promoter comparison in the 4- and 24-hour viral exposure experiments can be found in Table A3 and A4 respectively.

To assess if increasing the viral exposure time from 4- to 24-hours significantly increases the transduction efficiency, multiple-t tests were conducted for each promoter separately. The results indicated that 24-hours of viral exposure significantly increased the percentage of eGFP positive cells for each promoter in at least, but not limited to, the MOI range of 1-30. Except for SFFV, where the percentage of eGFP positive cells did not differ significantly at MOI 30 and EF1a for which a significant difference was only found between the MOI range of 3-10 (Table A5).

Transduction efficiency (live cell imaging)

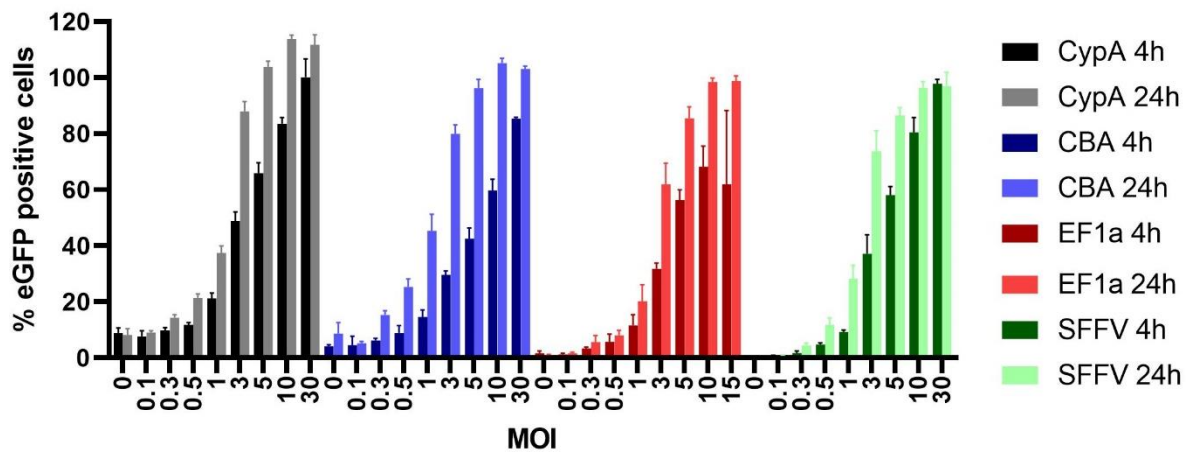


Figure 8: Viral titration of B4G12 cells with the different lentiviral vectors after 4- and 24-hours of viral exposure. The amount of eGFP positive cells, 58-hours after transduction, is shown for each MOI as determined based on the live cell imaging data (n=3). eGFP, enhanced green fluorescent protein; CypA, cyclophilin A; CBA, chimeric cytomegalovirus-chicken B-actin; EF1a, elongating factor-1a; SFFV, spleen focus-forming virus

4.2.2.2 Flow cytometry

To confirm the amount of eGFP positive cells as determined by live cell imaging analysis, flow cytometry was employed. A gating was performed (Fig. 9A) to isolate cells from debris and for each MOI individual histograms were generated. As example, the histogram of the 24-hour exposure to the SFFV promoter-containing vector is represented in Figure 9B. The histograms of all other promoters and exposure times can be found in the Appendix (Fig. A5 A-H). These histograms were used to determine the percentage of eGFP positive cells as depicted in Figure 10. Analogous to the live cell imaging data, an increase in MOI resulted in a higher percentage of eGFP positive cells and 4-hours of viral exposure led to an overall lower transduction efficiency compared to 24-hours of exposure.

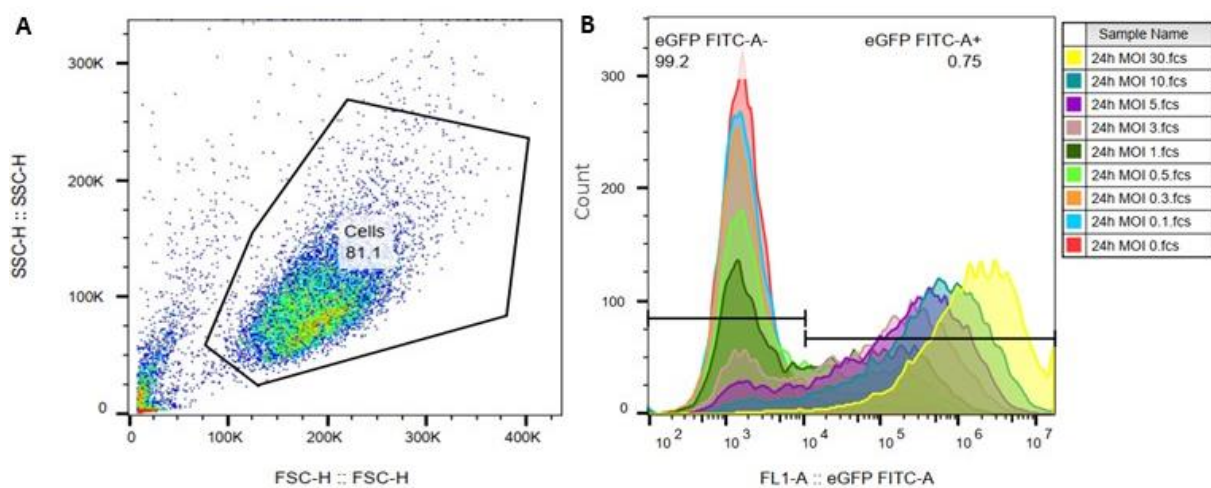


Figure 9: (A) Example of gating definition from a negative control displayed in a dot plot with the side scatter in function of forward scatter. (B) Example of flow cytometric readout from the SFFV-promoter titration after 24-hours of viral exposure with counts in function of green fluorescent intensity. SFFV, spleen focus-forming virus

Transduction efficiency (flow cytometry)

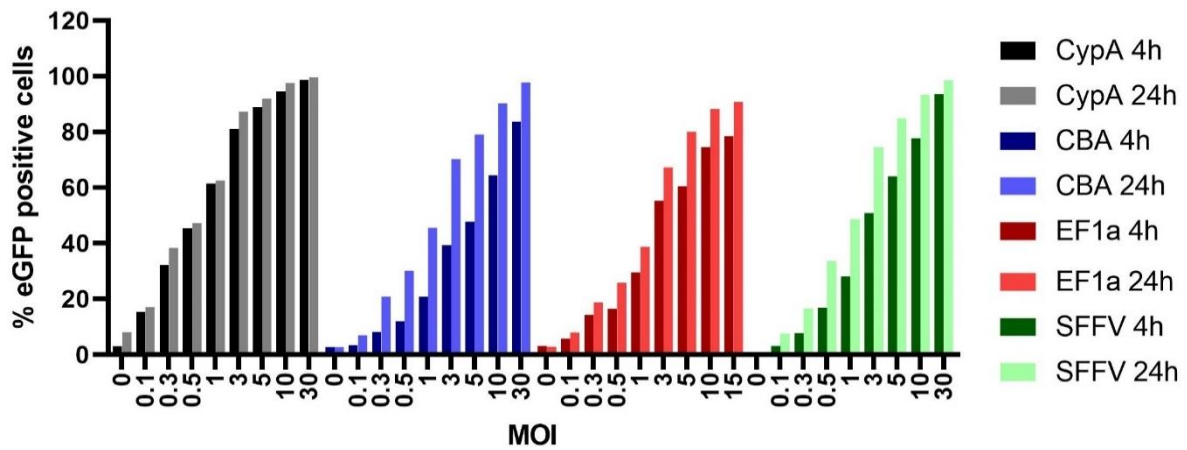


Figure 10: Viral titration of B4G12 cells with different lentiviral vectors after 4- and 24-hours of viral exposure. The amount of eGFP positive cells is determined by using flow cytometry ($n=1$). eGFP, enhanced green fluorescent protein; CypA, cyclophilin A; CBA, chimeric cytomegalovirus-chicken B-actin; EF1a, elongating factor-1a; SFFV, spleen focus-forming virus

4.2.3 eGFP expression intensity

Apart from the percentage of eGFP positive cells, the flow cytometric histograms (Fig. A5 A-H) can also be used to determine the mean eGFP expression intensity. Since a stronger promoter causes a higher eGFP expression intensity, this metric can be used to assess promoter strength. The results show that the SFFV promoter had the highest mean eGFP intensity compared to the other promoters which may indicate that it was the strongest of the promoters tested in this project (Fig. 11). However, more replicates are needed in order to do statistical testing and it should be confirmed that this effect is not caused by differences in copy number.

When the amount of eGFP positive cells was nearing 100%, the mean eGFP intensity continues to increase linearly (Fig. 12). This increase was most likely caused by the occurrence of multiple copy numbers per cell. A higher concentration of viruses increases the chance that the same cell is transduced multiple times. Hence, it is speculated that the high eGFP intensity observed with higher MOIs was a result of the presence of multiple copy numbers per cell.

Promoter strength

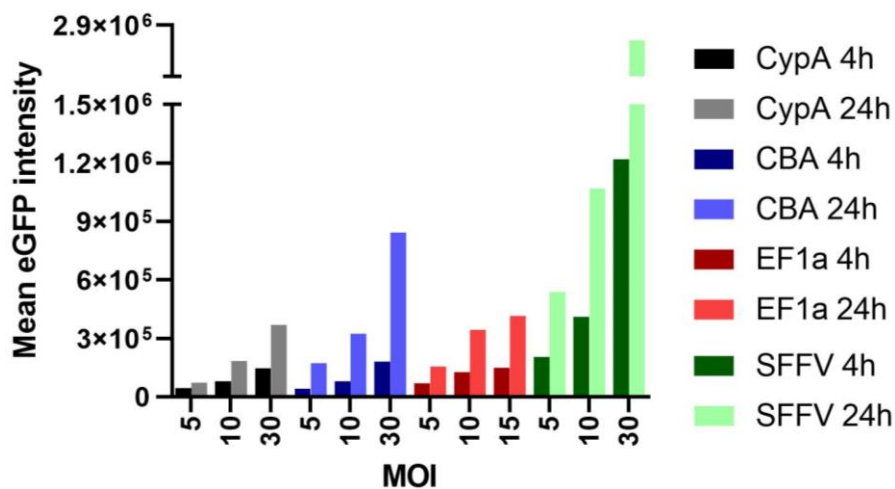


Figure 11: Mean eGFP intensity determined by flow cytometry for the highest MOIs of each vector in B4G12 cells ($n=1$). eGFP, enhanced green fluorescent protein; CypA, cyclophilin A; CBA, chimeric cytomegalovirus-chicken B-actin; EF1a, elongating factor-1a; SFFV, spleen focus-forming virus

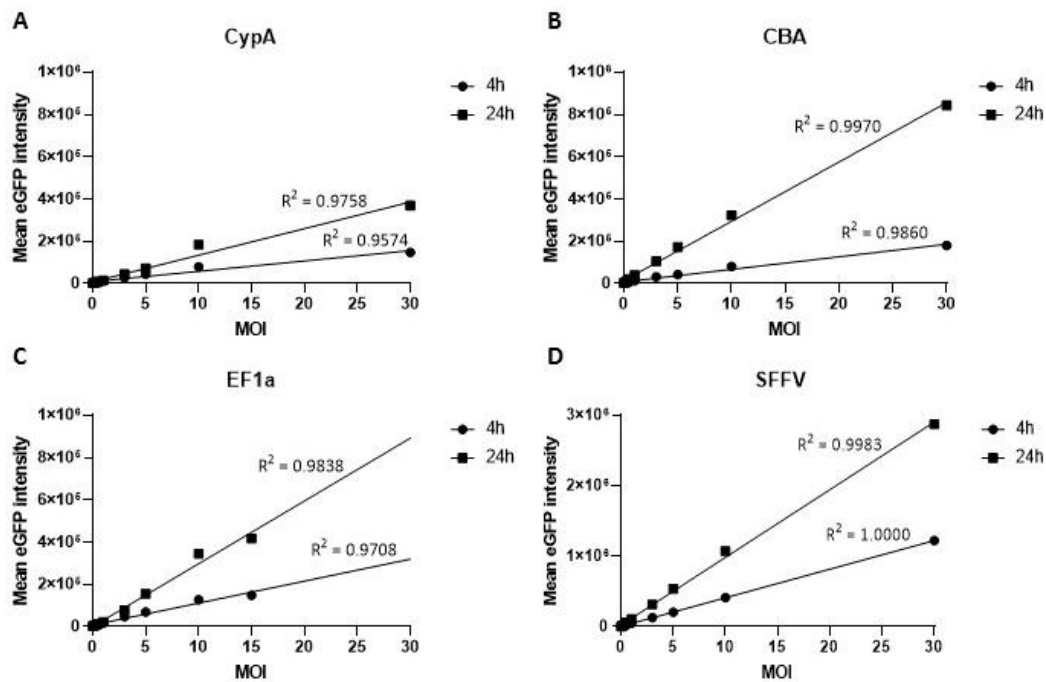


Figure 12: Linear correlation between the mean eGFP intensity and MOI for the 4- and 24-hour viral exposure experiment ($n=1$). eGFP, enhanced green fluorescent protein; CypA, cyclophilin A; CBA, chimeric cytomegalovirus-chicken B-actin; EF1a, elongating factor-1a; SFFV, spleen focus-forming virus

4.2.4 Toxicity of transduction

To determine the cytotoxic effect of lentiviral transduction, the data obtained by live cell imaging was fitted by using non-linear regression from which the population doubling times could be calculated for each vector (Figure A6 A-H). In case the effect of lentiviral transduction on population doubling time would only be modest in the range of MOI 0.1-30, an MOI of 100 was included in the SFFV-promoter experiments to give a better indication about its toxicity. The data showed that the population doubling time has an upward trend with increasing MOI and exposure time.

The population doubling time was compared between the different promoters in both the 4- and 24-hour viral exposure experiments. Statistical testing indicated that the SFFV promoter had a significantly lower population doubling time compared to the other promoters (mainly CBA) after both 4- and 24-hours of viral exposure (Table A6 and A7). However, since these significant differences also occur in the control, the observed decrease in population doubling time of SFFV is not promoter-related.

To assess if an increase in viral exposure time from 4- to 24-hours increased the population doubling time, multiple t-tests were performed for each promoter individually. The population doubling time was found to be significantly decreased in the 24-hour exposure experiment compared to 4-hour exposure experiment in CypA for MOI 0-10 (Table A8). However, since this significant difference was also found between the controls, this effect is not related to the difference in exposure times. Interestingly, a significant increase in population doubling time was found after 24-hours exposure to the constructs containing SFFV and CBA (Table A8). This indicates that long exposure to a high MOI is potentially more harmful for the cells compared to short exposure.

Lastly, within each promoter, it was assessed if some MOIs influence the population doubling time stronger than others. Only in the CypA 24-hour exposure experiment, a significant difference in population doubling time was found between MOI 3 and 30 (Fig. 13 B). However, a trend towards an increased population doubling time in the higher MOI range can also be observed in some of the other promoters (Fig. A6).

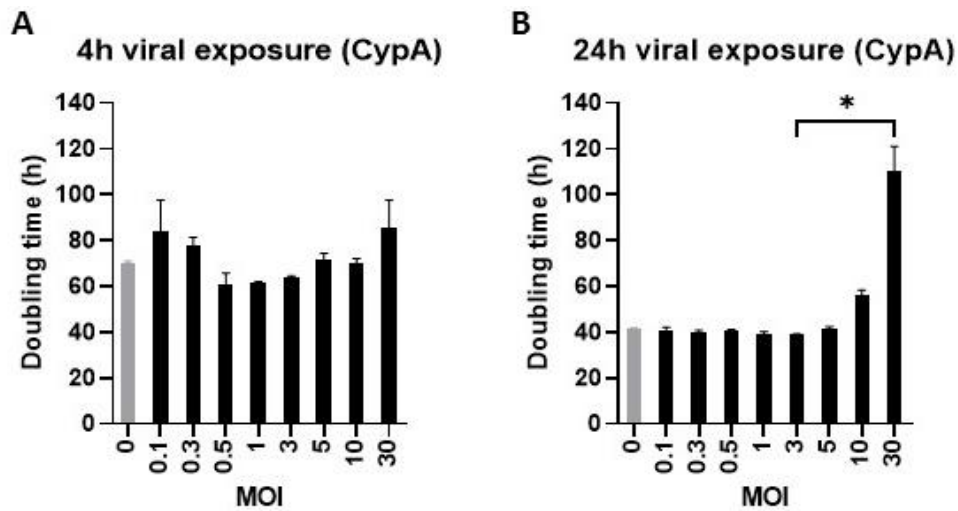


Figure 13: Population doubling time for the 4- and 24-hour lentiviral exposure experiment. Using a Kruskal-Wallis test followed by Dunn's multiple comparison test, a significant difference was found between MOI 3 and 30 in the 24-hour CypA experiment ($p = 0.0298$; $n=3$). CypA, cyclophilin A

4.2.5 PiggyBac transfection efficiency

Transfection by using an eGFP-containing PiggyBac vector did not result in eGFP positive B4G12 cells (Fig. 14). While nuclear staining with Nuclight Rapid Red reagent clearly indicated the presence of viable cells in the control (Fig. 14 A) and transfected condition (Fig. 14 B), there were no eGFP positive cells visible in the green channel (Fig. 14 D). This negative result was confirmed by employing flow cytometric analysis, where also no eGFP positive cells could be found (Fig. 15). It is assumed that this is caused by an extremely low transfection efficiency.

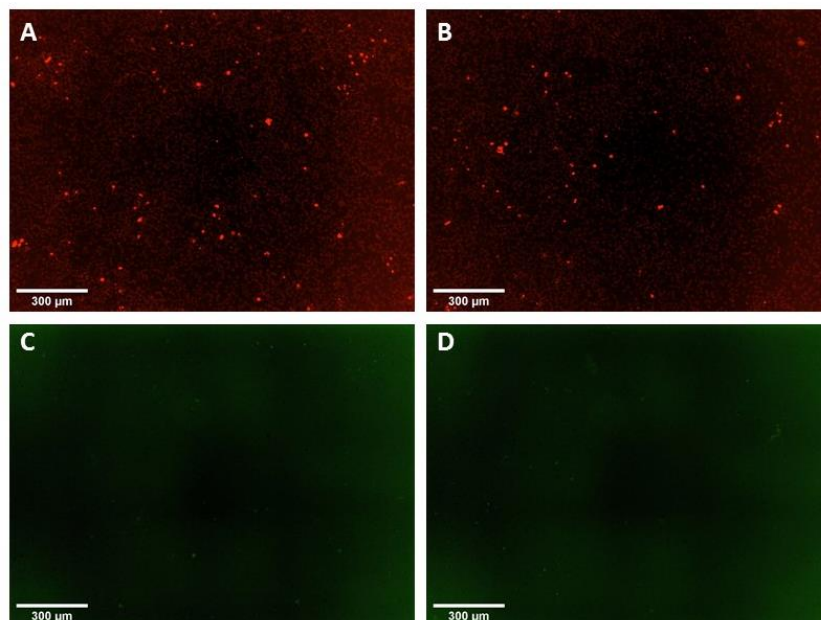


Figure 14: Images taken 66 hours after addition of PiggyBac vector, showing the red channel with Nuclight Rapid Red reagent stained nuclei in the control (A) and PiggyBac transfected cells (B). In the green channel, no eGFP positive cells were present in either the control (C) or PiggyBac transfected cells (D). eGFP, enhanced green fluorescent protein

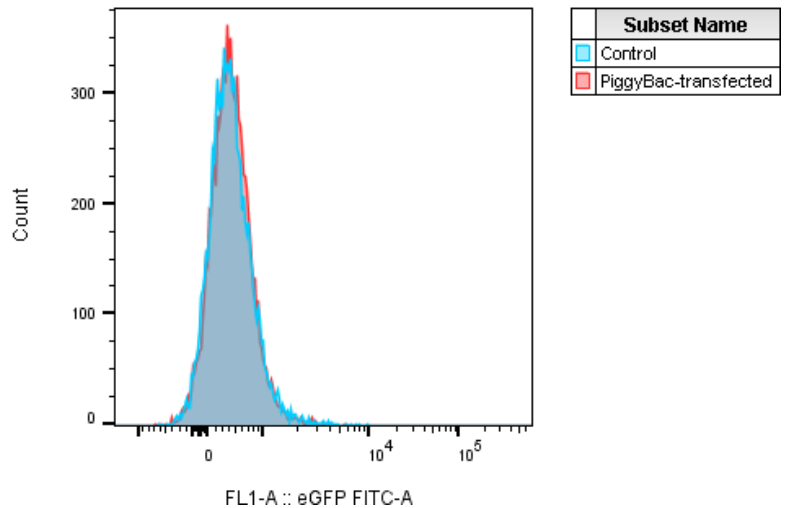


Figure 15: Flow cytometric data for the determination of eGFP-positive cells after transfection with the PiggyBac vector. eGFP, enhanced green fluorescent protein

4.3 Puromycin kill curve

4.3.1 Live cell imaging

After the cells were transfected with the PiggyBac vector or underwent viral transduction, the transduced/transfected cells need to be isolated from the unmodified cells. As previously mentioned, this will be done by ensuring puromycin resistance of the genetically modified cells through the addition of a puromycin resistance gene in the construct before insertion. The first step towards this puromycin selection was made by determining the lowest concentration that causes 100% lethality of B4G12 cells, termed LD₁₀₀.

The cells were exposed to different concentrations of puromycin (0-10 $\mu\text{g}/\text{mL}$). Nuclight Rapid Red reagent staining detected by live cell imaging allowed the monitoring of cell count throughout the experiment (Fig. 16). Since this nuclear staining does not disappear but gets more intense in dead cells, viable and non-viable cells were distinguished based on their difference in intensity. The percentage of viable cells was found to be at its minimum after 72-hours exposure to at least 2 $\mu\text{g}/\text{mL}$ puromycin. However, the curve indicates that not all cells are dead. When looking at the live cell images and their accompanying masks, it appeared that the software was not able to exclude all dead cells and contained some artifacts (see example in Fig. 16 B). Because it is essential to use the right concentration of puromycin when selecting construct-containing cells in the future, it was tried to confirm the results of this experiment by using another method.

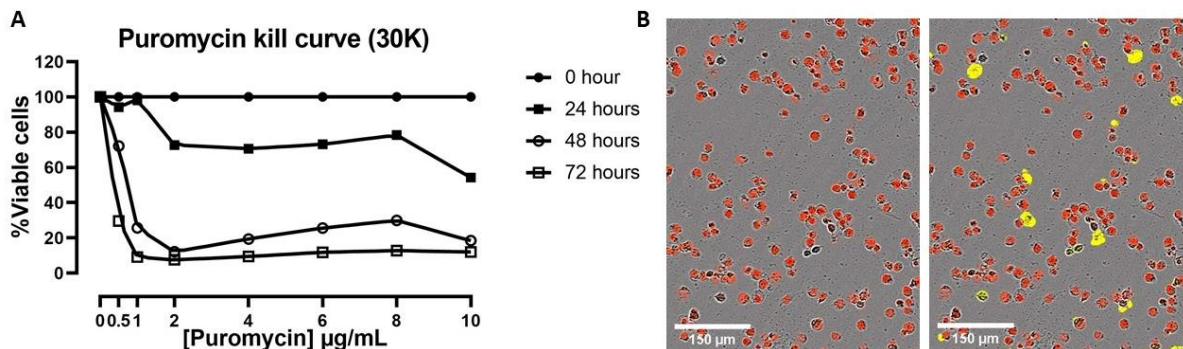


Figure 16: (A) Puromycin kill curve made with 30,000 B4G12 cells, showing the percentage of viable cells at different concentrations of puromycin after various times of exposure ($n=3$). (B) Phase-contrast and red channel image of Nuclight Rapid Red reagent stained cells at 10 $\mu\text{g}/\text{mL}$ puromycin after 72 hours of exposure (left) and its accompanying mask (yellow) made to detect viable cells mainly based on differences in fluorescent intensity (right).

4.3.2 Luminescence microplate reader

As an alternative to live cell imaging, the number of viable cells was assessed by using PrestoBlue staining which was performed every 24-hours for three days. In addition to the previous experiment, 30,000 and 75,000 cells were used to determine whether cell amount has an influence on the puromycin kill curve (Fig. 17 A and B). The percentage of viable cells when using 75,000 cells tended to be slightly higher compared to using 30,000 cells after 24- and 48-hours. However, for both cell numbers 72-hours of puromycin exposure caused 100% of the cells to die at 2 $\mu\text{g}/\text{mL}$ puromycin and above.

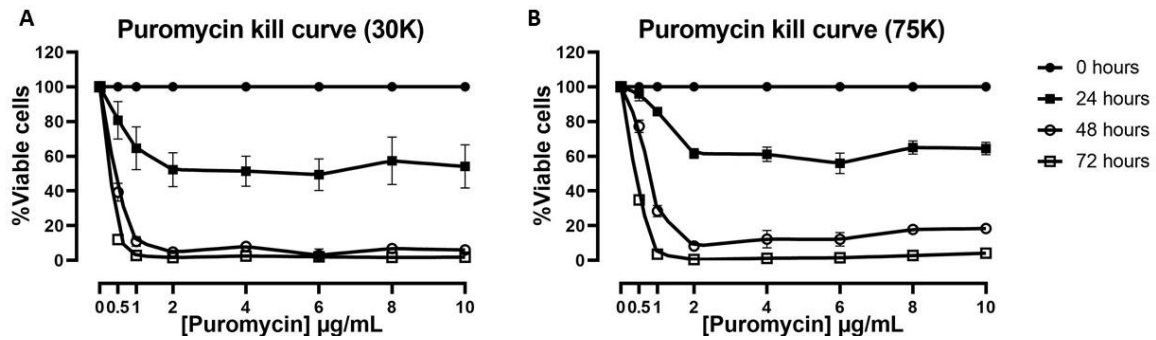


Figure 17: Puromycin kill curves used to determine the LD100 for 30,000 (A) and 75,000 (B) cells from a B4G12 cell line. The amount of viable cells was determined with PrestoBlue ($n=3$).

5 Discussion

5.1 Construct integration

5.1.1 Influence of multiplicity of infection, promoter and exposure time on transduction efficiency

5.1.1.1 Multiplicity of infection

In this project, lentiviral titration was performed on a B4G12 cell line by exposing the cells to an MOI range of 0-30 for 4- and 24-hours. The MOI range used for the titration was ideal to determine the viral concentration needed to obtain a transduced cell yield between 0 to 100%. Based on the flow cytometric data, the desired transduced cell yield of 20-30% can be acquired by using an MOI between 0.3 and 1, depending on the promoter and exposure time. Overall, a lower MOI would be preferred since this would be more cost-efficient and decrease the chance of obtaining high copy numbers.

5.1.1.2 Promoter

When comparing the percentage of eGFP positive cells between the different promoters (i.e. CypA, CBA, EF1a and SFFV), the transduction efficiency of the CypA-containing vector was significantly higher compared to some of the other promoters in the 4-hour viral exposure experiment at certain MOIs (Table A3). However, these differences were found in the control and lower MOI range which makes them less likely to be promoter-dependent. Since also the flow cytometric data indicates a higher transduction efficiency of the CypA promoter, a literature search was performed to find possible causes for this increased transduction efficiency (Fig. 10). There are a few factors that could cause variation in transduction efficiency between the different constructs in general. Firstly, it was found that differences in vector size of only a few 100 bp are enough to significantly decrease lentiviral transduction efficiency [75]. Secondly, the vector might get successfully transduced but an inefficiently functioning promoter could cause the transduction efficiency to appear low [76]. Finally, differences in promoter kinetics combined with an early assessment of transduction efficiency might also result in an apparently lower amount of eGFP positive cells. However, since the CypA-containing construct is about the same size compared to the other constructs, the eGFP intensity indicated that it was not stronger than the other promoters and its kinetics do not appear to be different, none of them can explain the observed significant difference in the 4-hour exposure experiments. Additional testing will be needed to elucidate whether this effect persists with a larger sample size.

Also in the 24-hour experiment some significant differences were found between CypA and some of the other promoters at specific MOIs (Table A4). The possible underlying causes mentioned above (i.e. lower construct size, higher promoter strength or deviations in kinetics) are not the cause. As such, more experiments will need to determine whether this difference will persist.

5.1.1.3 Exposure time

Statistical testing indicated that the percentage of eGFP positive cells is significantly higher after 24-hours compared to 4-hours of viral exposure in the middle-high MOI range (Table A5). Hence, the same yield of transduced cells can be obtained at lower MOIs if the viral exposure time is increased. Absence of significance between both exposure times in the lower MOIs is probably caused by the high standard deviation in relation to the percentage eGFP positive cells.

5.1.2 Comparative analysis between live cell imaging analysis and flow cytometry to determine the percentage of eGFP positive cells

In order to estimate the amount of eGFP positive cells, both live cell imaging analysis and flow cytometry were performed after transduction/transfection. The main purpose for using these methods was to assess if the accuracy of live cell imaging was comparable with this of flow cytometry. This way, the latter can be abandoned in future experiments since its destructive nature makes it less advantageous compared to live cell imaging.

The percentage difference was calculated between both methods for the 4- and 24-hour exposure experiment separately (Table 1). From this data, it is apparent that the live cell imaging analysis underestimates the amount of eGFP positive cells in the lower MOIs while its accuracy increases with an increasing MOI and exposure time. Indeed, the large difference in eGFP intensity between the lower and higher MOIs make it difficult to make a mask that fits the entire eGFP intensity range. Additional finetuning of the mask and more experimental data is needed before live cell imaging analysis can fully replace flow cytometry for the quantification of eGFP positive cells. Making a mask for a smaller eGFP intensity range might also make quantification with live cell imaging more accurate.

Table 1: Average percentage difference of the percentage eGFP positive cells for all promoters estimated with live cell imaging in relation to the values determined with flow cytometry in the 4- and 24-hour viral exposure experiment (MOI 30 was only calculated with the values for CypA, CBA and SFFV). eGFP, enhanced green fluorescent protein; CypA, cyclophilin A; CBA, chimeric cytomegalovirus-chicken B-actin; EF1a, SFFV, spleen focus-forming virus

MOI	Percentage difference (%)	
	4-hour	24-hour
0	26.0	13.0
0.1	-43.4	-60.0
0.3	-61.9	-58.1
0.5	-59.3	-51.1
1	-55.7	-32.5
3	-33.5	1.4
5	-13.2	10.8
10	-5.9	12.0
30	2.6	5.4

5.1.3 Relation between the observed transduction efficiency and literature

To assess the transduction efficiency of the B4G12 cell line compared to a highly permissive cell line (i.e. HeLa) and primary HCEncs, a literature search was conducted. The overall transduction efficiency of the B4G12 cell line was similar to this of the highly permissive HeLa cell line (Table 2) [77]. When comparing the transduction efficiency between the B4G12 cell line and primary HCEncs, the B4G12 cells appear to be more prone to viral transduction [78]. However, the MOI for the primary HCEncs was calculated only based on the amount of corneal endothelial cells while the entire cornea was exposed to the virus. This probably causes the MOI of 30 to be overestimated which explains the large difference between the transduction efficiency of primary HCEncs and B4G12 cells. Because of the relatively high transduction efficiency in both primary and immortalised corneal endothelial cells, transduction increasing reagents (e.g. polybrene) will probably not be needed in the future.

Table 2: Comparison of the cell transduction yield determined by flow cytometry in this project (average of promoters, 24-hours viral exposure) with data found in literature concerning the HeLa cell line and primary human corneal endothelial cells (HCEncs).

Cell type	Transduced cell yield (%)		
	MOI 1	MOI 10	MOI 30
B4G12	49	92	99
HeLa [77]	40	95	100
Primary HCEncs [78]	NA	NA	35

5.1.4 Determining the strongest promoter

A major milestone to obtain reversible immortalisation in the future, will be increasing the proliferative capacity of corneal endothelial cells by the introduction of an oncogene. In order to get a high expression of this oncogene, a promoter that drives strong gene expression in corneal endothelial cells will be needed. In this project, the strength of each promoter was assessed on the basis of the mean eGFP intensity. From all promoters that were tested, SFFV turned out to be the strongest (Fig. 11). However, as mentioned earlier, a qPCR analysis will need to confirm that this is not caused by differences in gene copy number. When comparing these results to literature, the strength of SFFV seemed to be cell type dependent [79,80]. In general, it is considered to be a strong viral promoter regularly used to drive expression of genes in different cell types (e.g. hematopoietic cells) [80,81]. Additional experiments will be needed to assess whether this promoter can drive constitutive gene expression on the long term without being silenced [82].

If the SFFV promoter is used for further experiments, the flow cytometric data indicates that 24-hours of exposure to an MOI of 0.5 will result in the desired transduced cell yield of 20-30%.

5.1.5 Toxicity of viral transduction

To compare the toxicity of lentiviral transduction in general and between the different promoter constructs, the population doubling times were determined for each MOI. In the SFFV promoter experiment the population doubling time was found to be significantly lower compared to some of the other promoters at specific MOI's (Table A6 and A7). However, as previously mentioned, this is not thought to be a promoter-related effect as also the control has a relatively low population doubling time in the SFFV promoter experiment. Possibly, the seeding density was lower in this experiment causing the cells to experience less contact inhibition and grow faster.

Results also indicated a trend towards increased population doubling time with increasing MOI and exposure time. This suggest that high MOI (≥ 10) could confer some cytotoxicity to HCEncs. The effect seems to be more pronounced with CBA and SFFV since the population doubling time was found to be significantly higher after 24-hours exposure compared to 4-hours exposure at MOI 30 (Table A8). However, this does not influence the choice of promoter or MOI in this project because it only occurs at high viral concentrations. Growth inhibiting effects were also reported in other cell types upon lentiviral transduction, albeit less pronounced as observed here [83,84]. Because no mock transduction was executed, a possible influence of high eGFP expression on cell fitness and image acquisition cannot be ruled out [85].

5.1.6 Transfection of the PiggyBac vector

The introduction of a fully removable construct by using a PiggyBac vector is an important alternative for viral transduction to increase the safety of the reversible immortalised cells in the future. Unfortunately, no eGFP positive cells have been detected after transfection with the PiggyBac vector (Fig. 14 and 15). Most likely, this is caused by an extremely low transfection efficiency. Future testing will comprise transfection of a HEK293 cell line to assess if the low transfection efficiency is cell type dependent.

If transfection of the HEK293 cell line is successful, the Purefection transfection reagent might not be compatible with the B4G12 cell line. Another lipofection reagents that could be used instead is Lipofectamine 2000 (Thermofisher) since it has already been successfully used in B4G12 cells according to literature [86].

5.2 LD₁₀₀ of puromycin in the B4G12 cell line

To ensure a homogeneous population of cells containing the construct, an antibiotics selection will need to be performed. Data obtained through a PrestoBlue staining indicated that the LD₁₀₀ of B4G12 cells was reached at 2 µg/mL puromycin both for 30,000 and 75,000 cells (Fig. 17). This is in line with the concentration of puromycin used in other adherent cell lines [87]. For primary corneal endothelial cells, exposure to a concentration of 1 µg/mL puromycin for 7 days has been reported [33]. Evaluation of the determined LD₁₀₀ and exposure time on puromycin resistant B4G12 cells will be needed. If the proposed selection condition turns out to be too extreme, additional experiments will be needed with a longer evaluation of cell viability than the one presented in this project.

6 Conclusion and perspectives

In this project, the B4G12 cell line was successfully transduced by using lentiviral vectors with different promoters. The desired transduction efficiency of 20-30% can be obtained by using an MOI between 0.3 and 1 depending on the construct that was inserted and the time of viral exposure. Overall, a longer exposure to the viral vectors resulted in a higher amount of transduced cells. The SFFV promoter resulted in the highest mean eGFP intensity and is therefore considered to drive eGFP expression the strongest. For this construct, 24-hour exposure to an MOI of 0.5 is preferred to obtain the desired percentage of transduced cells.

Unfortunately, no eGFP positive cells were detected after transfection of the PiggyBac vector. Additional experiments will be needed to determine whether this is caused by a low transfection efficiency or an incompatibility between the B4G12 cell line and the PureFection transfection reagent.

To select puromycin resistant B4G12 cells in the future, it was determined that the LD₁₀₀ of unmodified B4G12 cells was found to be 72-hour exposure to 2 µg/ml puromycin. However, increasing the exposure time to reduce the dose of puromycin might be preferred when transitioning to primary HCEncs.

The different experiments performed in this master's thesis are part of the foundation to accomplish the reversible immortalisation of HCEncs. While it mainly focussed on gene introduction and puromycin-mediated selection in the B4G12 immortalised cell line, also the evaluation of the different gene excision mechanisms and validation in primary HCEncs are paramount to continue this project.

Bibliography

1. Meek KM, Knupp C. Corneal structure and transparency. *Prog Retin Eye Res.* 2015;49:1–16.
2. Eghrari AO, Riazuddin SA, Gottsch JD. Overview of the Cornea: Structure, Function, and Development. 1st ed. Vol. 134, *Progress in Molecular Biology and Translational Science.* Elsevier Inc.; 2015. 7–23 p.
3. Feizi S, Jafarinasab MR, Karimian F, Hasanpour H, Masudi A. Central and peripheral corneal thickness measurement in normal and keratoconic eyes using three corneal pachymeters. *J Ophthalmic Vis Res.* 2014;9(3):296.
4. Mochizuki H, Fukui M, Hatou S, Yamada M, Tsubota K. Evaluation of ocular surface glycocalyx using lectin-conjugated fluorescein. *Clin Ophthalmol.* 2010;4(1):925–30.
5. Schermer A, Galvin S, Sun TT. Differentiation-related expression of a major 64K corneal keratin in vivo and in culture suggests limbal location of corneal epithelial stem cells. *J Cell Biol.* 1986;103(1):49–62.
6. Thoft RA, Friend J. The X, Y, Z hypothesis of corneal epithelial maintenance. *Invest Ophthalmol Vis Sci.* 1983;24:1442–3.
7. Hayashi S, Osawa T, Tohyama K. Comparative observations on corneas, with special reference to Bowman's layer and Descemet's membrane in mammals and amphibians. *J Morphol.* 2002;254(3):247–58.
8. Peh GSL, Beuerman RW, Colman A, Tan DT, Mehta JS. Human corneal endothelial cell expansion for corneal endothelium transplantation: An overview. *Transplantation.* 2011;91(8):811–9.
9. Torricelli AAM, Wilson SE. Cellular and extracellular matrix modulation of corneal stromal opacity. *Exp Eye Res.* 2014;129(October):151–60.
10. DelMonte DW, Kim T. Anatomy and physiology of the cornea. *J Cataract Refract Surg.* 2011;37(3):588–98.
11. Matthyssen S, Van den Bogerd B, Dhubhghaill SN, Koppen C, Zakaria N. Corneal regeneration: A review of stromal replacements. *Acta Biomater.* 2018;
12. Bonanno JA. Molecular mechanisms underlying the corneal endothelial pump. *Exp Eye Res.* 2012;95(1):2–7.
13. Ali M, Raghunathan VK, Li JY, Murphy CJ, Thomasy SM. Biomechanical relationships between the corneal endothelium and Descemet's membrane. *Exp Eye Res.* 2016;152:57–70.
14. Joyce NC. Proliferative capacity of the corneal endothelium. *Prog Retin Eye Res.* 2003;22(3):359–89.
15. Waring GO, Bourne WM, Edelhauser HF, Kenyon KR. The Corneal Endothelium: Normal and Pathologic Structure and Function. *Ophthalmology.* 1982;89(6):531–90.
16. Bonanno JA. Identity and regulation of ion transport mechanisms in the corneal endothelium. *Prog Retin Eye Res.* 2003;22(1):69–94.
17. Elbaz U, Mireskandari K, Tehrani N, Shen C, Khan MS, Williams S, et al. Corneal endothelial cell density in children: normative data from birth to 5 years old. *Am J Ophthalmol.* 2017;173:134–8.
18. Abdellah MM, Ammar HG, Anbar M, Mostafa EM, Farouk MM, Sayed K, et al. Corneal Endothelial Cell Density and Morphology in Healthy Egyptian Eyes. *J Ophthalmol.* 2019;2019(Cd).

19. Bourne WM, Nelson LR, Hodge DO. Central corneal endothelial cell changes over a ten-year period. *Invest Ophthalmol Vis Sci.* 1997;38(3):779–82.
20. Van den Bogerd B, Dhubhghaill SN, Koppen C, Tassignon MJ, Zakaria N. A review of the evidence for in vivo corneal endothelial regeneration. *Surv Ophthalmol.* 2018;63(2):149–65.
21. Joyce NC, Meklir B, Joyce SJ, Zieske JD. Cell cycle protein expression and proliferative status in human corneal cells. *Investig Ophthalmol Vis Sci.* 1996;37(4):645–55.
22. Joyce NC. Proliferative capacity of corneal endothelial cells. *Exp Eye Res.* 2012;95(1):16–23.
23. McAlister JC, Joyce NC, Harris DL, Ali RR, Larkin DFP. Induction of replication in human corneal endothelial cells by E2F2 transcription factor cDNA transfer. *Investig Ophthalmol Vis Sci.* 2005;46(10):3597–603.
24. Wilson SE, Weng J, Blair S, He YG, Lloyd S. Expression of E6/E7 or SV40 large T antigen-coding oncogenes in human corneal endothelial cells indicates regulated high-proliferative capacity. *Investig Ophthalmol Vis Sci.* 1995;36(1):32–40.
25. Wilson SE, Lloyd SA, He YG, McCash CS. Extended life of human corneal endothelial cells transfected with the SV40 large T antigen. *Investig Ophthalmol Vis Sci.* 1993;34(6):2112–23.
26. Feizi S. Corneal endothelial cell dysfunction: etiologies and management. *Ther Adv Ophthalmol.* 2018;10:2515841418815802.
27. Gain P, Jullienne R, He Z, Aldossary M, Acquart S, Cognasse F, et al. Global survey of corneal transplantation and eye banking. *JAMA Ophthalmol.* 2016;134(2):167–73.
28. Bourne WM. Biology of the corneal endothelium in health and disease. *Eye.* 2003;17(8):912–8.
29. Elhalis H, Azizi B, Jurkunas U V. Fuchs endothelial corneal dystrophy. *Ocul Surf.* 2010;8(4):173–84.
30. Jurkunas U V, Bitar M, Rawe I. Colocalization of Increased Transforming Growth Factor- Beta – Induced Protein (TGFBIp) and Clusterin in Fuchs Endothelial Corneal Dystrophy. 2009;50(3):1–8.
31. Ramboer E, De Craene B, De Kock J, Vanhaecke T, Berx G, Rogiers V, et al. Strategies for immortalization of primary hepatocytes. *J Hepatol.* 2014;61(4):925–43.
32. Wang Y, Chen S, Yan Z, Pei M. A prospect of cell immortalization combined with matrix microenvironmental optimization strategy for tissue engineering and regeneration 06 Biological Sciences 0601 Biochemistry and Cell Biology. *Cell Biosci.* 2019;9(1):1–21.
33. Schmedt T, Chen Y, Nguyen TT, Li S, Bonanno JA, Jurkunas U V. Telomerase Immortalization of Human Corneal Endothelial Cells Yields Functional Hexagonal Monolayers. *PLoS One.* 2012;7(12):1–11.
34. Salmon P, Oberholzer J, Occhiodoro T, Morel P, Lou J, Trono D. Reversible immortalization of human primary cells by lentivector-mediated transfer of specific genes. *Mol Ther.* 2000;2(4):404–14.
35. Chira S, Jackson CS, Oprea I, Ozturk F, Pepper MS, Diaconu I, et al. Progresses towards safe and efficient gene therapy vectors. *Oncotarget.* 2015;6(31):30675–703.
36. Ginn SL, Amaya AK, Alexander IE, Edelstein M, Abedi MR. Gene therapy clinical trials worldwide to 2017: An update. *J Gene Med.* 2018;20(5).

37. Sakuma T, Barry MA, Ikeda Y. Lentiviral vectors: Basic to translational. *Biochem J.* 2012;443(3):603–18.
38. Naldini L, Blömer U, Gallay P, Ory D, Mulligan R, Gage FH, et al. In vivo gene delivery and stable transduction of nondividing cells by a lentiviral vector. *Science (80-).* 1996;272(5259):263–7.
39. Zufferey R, Nagy D, Mandel RJ, Naldini L, Trono D. Multiply attenuated lentiviral vector achieves efficient gene delivery in vivo. *Nat Biotechnol.* 1997;15(9):871–5.
40. Dull T, Zufferey R, Kelly M, Mandel RJ, Nguyen M, Trono D, et al. A third-generation lentivirus vector with a conditional packaging system. *J Virol.* 1998;72(11):8463–71.
41. Yu SF, von Ruden T, Kantoff PW, Garber C, Seiberg M, Rütther U, et al. Self-inactivating retroviral vectors designed for transfer of whole genes into mammalian cells. *Proc Natl Acad Sci U S A.* 1986;83(10):3194–8.
42. Schlimgen R, Howard J, Wooley D, Thompson M, Baden LR, Yang OO, et al. Risks associated with lentiviral vector exposures and prevention strategies. *J Occup Environ Med.* 2016;58(12):1159–66.
43. Hoess RH, Wierzbicki A, Abremski K. The role of the loxP spacer region in PI site-specific recombination. *Nucleic Acids Res.* 1986;14(5):2287–300.
44. Abremski K, Hoess R, Sternberg N. Studies on the properties of P1 site-specific recombination: Evidence for topologically unlinked products following recombination. *Cell.* 1983;32(4):1301–11.
45. abm. Cre-Lox Recombination [Internet]. [cited 2019 Dec 19]. Available from: https://www.abmgood.com/marketing/knowledge_base/Cre-Lox_Recombination.php
46. Izsvák Z, Ivics Z. Sleeping Beauty transposition: Biology and applications for molecular therapy. *Mol Ther.* 2004;9(2):147–56.
47. Fraser MJ, Ciszczon T, Elick T, Bauser C. Precise excision of TTAA-specific lepidopteran transposons piggyBac (IFP2) and tagalong (TFP3) from the baculovirus genome in cell lines from two species of Lepidoptera. *Insect Mol Biol.* 1996;5(2):141–51.
48. Yusa K. piggyBac transposon. In: *Mobile DNA III.* American Society of Microbiology; 2015. p. 875–92.
49. Vargas JE, Chicaybam L, Stein RT, Tanuri A, Delgado-Cañedo A, Bonamino MH. Retroviral vectors and transposons for stable gene therapy: Advances, current challenges and perspectives. *J Transl Med.* 2016;14(1):1–15.
50. Li X, Burnight ER, Cooney AL, Malani N, Brady T, Sander JD, et al. PiggyBac transposase tools for genome engineering. *Proc Natl Acad Sci U S A.* 2013;110(25).
51. Ding S, Wu X, Li G, Han M, Zhuang Y, Xu T. Efficient transposition of the piggyBac (PB) transposon in mammalian cells and mice. *Cell.* 2005;122(3):473–83.
52. Li MA, Turner DJ, Ning Z, Yusa K, Liang Q, Eckert S, et al. Mobilization of giant piggyBac transposons in the mouse genome. *Nucleic Acids Res.* 2011;39(22).
53. Li MA, Pettitt SJ, Eckert S, Ning Z, Rice S, Cadinanos J, et al. The piggyBac Transposon Displays Local and Distant Reintegration Preferences and Can Cause Mutations at Noncanonical Integration Sites. *Mol Cell Biol.* 2013;33(7):1317–30.
54. Gogol-Doring A, Ammar I, Gupta S, Bunse M, Miskey C, Chen W, et al. Genome-wide profiling reveals remarkable parallels between insertion site selection properties of the MLV retrovirus and the piggyBac transposon in primary human CD4+ T cells. *Mol Ther.* 2016;24(3):592–606.

55. Fang SY, Hu CQ, Liu MN, Tao L, Wang Y, Gong MJ, et al. Reversibly immortalized hepatic progenitor cell line containing double suicide genes. *Int J Mol Med*. 2018;42(4):1977–86.
56. Jones BS, Lamb LS, Goldman F, Di Stasi A. Improving the safety of cell therapy products by suicide gene transfer. *Front Pharmacol*. 2014;5(November):1–8.
57. Vassaux G. Use of suicide genes for cancer gene therapy : study of the. *Expert Opin Biol Ther*. 2004;4(4):519–30.
58. Yu S, Yi M, Qin S, Wu K. Next generation chimeric antigen receptor T cells: Safety strategies to overcome toxicity. *Mol Cancer*. 2019;18(1).
59. Springer CJ, Niculescu-Duvaz I. Gene-directed enzyme prodrug therapy (GDEPT): choice of prodrugs. *Adv Drug Deliv Rev*. 1996;22(3):351–64.
60. Zhang J, Kale V, Chen M. Gene-Directed Enzyme Prodrug Therapy. *AAPS J*. 2015;17(1):102–10.
61. Karjoo Z, Chen X, Hatefi A. Progress and problems with the use of suicide genes for targeted cancer therapy. *Adv Drug Deliv Rev*. 2016;99:113–28.
62. MolMed SpA. Assessment report Zalmoxis [Internet]. 2016. Available from: https://www.ema.europa.eu/en/documents/assessment-report/zalmoxis-epar-public-assessment-report_en.pdf
63. MolMed SpA. MolMed Press Release [Internet]. 2019 [cited 2019 Dec 9]. Available from: [https://www.molmed.com/sites/default/files/2019-10/PR_Zalmoxis update WITHDRAWAL_101019_DEF.pdf](https://www.molmed.com/sites/default/files/2019-10/PR_Zalmoxis_update_WITHDRAWAL_101019_DEF.pdf)
64. European Commission. Union Register of not active medicinal products for human use [Internet]. 2019 [cited 2019 Dec 9]. Available from: <https://ec.europa.eu/health/documents/community-register/html/h1121.htm>
65. Fan L, Freeman KW, Khan T, Pham E, Spencer DM. Improved artificial death switches based on caspases and FADD. *Hum Gene Ther*. 1999;10(14):2273–85.
66. Gargett T, Brown MP. The inducible caspase-9 suicide gene system as a “safety switch” to limit on-target, off-tumor toxicities of chimeric antigen receptor T-cells. *Front Pharmacol*. 2014;5(OCT):1–7.
67. Kemper K, Rodermond H, Colak S, Grandela C, Medema JP. Targeting colorectal cancer stem cells with inducible caspase-9. *Apoptosis*. 2012;17(5):528–37.
68. Philip B, Kokalaki E, Mekkaoui L, Thomas S, Straathof K, Flutter B, et al. A highly compact epitope-based marker/suicide gene for easier and safer T-cell therapy. *Blood*. 2014;124(8):1277–87.
69. Wang X, Chang WC, Wong CLW, Colcher D, Sherman M, Ostberg JR, et al. A transgene-encoded cell surface polypeptide for selection, in vivo tracking, and ablation of engineered cells. *Blood*. 2011;118(5):1255–63.
70. Introna M, Barbui AM, Bambacioni F, Casati C, Gaipa G, Borleri G, et al. Genetic modification of human T cells with CD20: A strategy to purify and lyse transduced cells with anti-CD20 antibodies. *Hum Gene Ther*. 2000;11(4):611–20.
71. Rönkkö S, Vellonen KS, Järvinen K, Toropainen E, Urtti A. Human corneal cell culture models for drug toxicity studies. *Drug Deliv Transl Res*. 2016;6(6):660–75.
72. Peh GSL, Toh KP, Wu FY, Tan DT, Mehta JS. Cultivation of human corneal endothelial cells isolated from paired donor corneas. *PLoS One*. 2011;6(12).
73. Picot J, Guerin CL, Le Van Kim C, Boulanger CM. Flow cytometry: Retrospective, fundamentals and recent instrumentation. *Cytotechnology*. 2012;64(2):109–30.
74. Horizon Discovery. Dose response curve for antibiotic selection of mammalian cells (kill curve) [Internet]. Cambridge; 2018. p. 1. Available from:

<https://horizondiscovery.com/-/media/Files/Horizon/resources/Protocols/antibiotic-kill-curve-protocol.pdf>

75. Barrett KC, Mendes RD, Smits WK, Wijk YMVH Van, Pieters R, Meijerink JPP. Lentiviral gene transfer into human and murine hematopoietic stem cells: size matters. *BMC Res Notes*. 2016;1–6.
76. Ikeda Y, Collins MKL, Radcliffe PA, Mitrophanous KA, Takeuchi Y. Gene transduction efficiency in cells of different species by HIV and EIAV vectors. *Gene Ther*. 2002;9(14):932–8.
77. Nguyen TH, Oberholzer J, Birraux J, Majno P, Morel P, Trono D. Highly efficient lentiviral vector-mediated transduction of nondividing, fully reimplantable primary hepatocytes. *Mol Ther*. 2002;6(2):199–209.
78. Parker DGA, Kaufmann C, Brereton HM, Anson DS, Jessup CF, Marshall K. Lentivirus-mediated gene transfer to the rat , ovine and human cornea. 2007;(14):760–7.
79. Oellig C, Seliger B. Gene Transfer Into Brain Tumor Cell Lines: Reporter Gene Expression Using Various Cellular and Viral Promoters. 1990;396:390–6.
80. Su R, Baylink DJ, Neises A, Kiroyan JB, Meng X, Payne KJ, et al. Efficient Generation of Integration-Free iPS Cells from Human Adult Peripheral Blood Using BCL-XL Together with Yamanaka Factors. 2013;8(5).
81. Benabdellah K, Cobo M, Muñoz P, Toscano MG, Martin F. Development of an all-in-one lentiviral vector system based on the original TetR for the easy generation of Tet-on cell lines. *PLoS One*. 2011;6(8).
82. Ellis J. Silencing and variegation of gammaretrovirus and lentivirus vectors. *Hum Gene Ther*. 2005;16(11):1241–6.
83. Lee CI, Kohn DB, Ekert JE, Tarantal AF. Morphological Analysis and Lentiviral Transduction of Fetal Monkey Bone Marrow-Derived Mesenchymal Stem Cells. *Mol Ther*. 2004;9(1):112–23.
84. Schott JW, Jaeschke NM, Hoffmann D, Maetzig T, Ballmaier M, Godinho T, et al. Deciphering the Impact of Parameters Influencing Transgene Expression Kinetics after Repeated Cell Transduction with Integration-Deficient Retroviral Vectors. 2015;405–18.
85. Baens M, Noels H, Broeckx V, Hagens S, Fevery S, Billiau AD, et al. The Dark Side of EGFP: Defective Polyubiquitination. 2006;2(1):1–6.
86. Hsueh YJ, Chen HC, Wu SE, Wang TK, Chen JK, Ma DHK. Lysophosphatidic acid induces YAP-promoted proliferation of human corneal endothelial cells via PI3K and ROCK pathways. *Mol Ther - Methods Clin Dev*. 2015;2(March):15014.
87. ThermoFisher. Puromycin [Internet]. [cited 2020 Apr 13]. Available from: <https://www.thermofisher.com/be/en/home/life-science/cell-culture/transfection/selection/puromycin.html>
88. ThermoFisher. Viral vector [Internet]. [cited 2019 Dec 29]. Available from: <https://www.thermofisher.com/be/en/home/references/gibco-cell-culture-basics/transfection-basics/gene-delivery-technologies/viral-delivery/viral-vectors.html>
89. Leibniz Institute DSMZ. HCEC-B4G12 [Internet]. [cited 2020 Jan 6]. Available from: <https://www.dsmz.de/collection/catalogue/details/culture/ACC-647>
90. Janson B. Encyclopedia of Ophthalmology. *Encycl Ophthalmol*. 2016;2006–7.
91. System Biosciences. PiggyBac Transposon Vector System: User Manual. Vol. 14. 2018.

Appendix

Table A1: Overview of the most common viral vector systems with their main characteristics [88].

Viral vector	Size	DNA cargo size	Infection	Expression
Adenovirus	36 kb (dsDNA)	8 kb	Dividing and non-dividing cells	Transient
Retrovirus	7-11 kb (ssRNA)	8kb	Dividing cells	Stable
Lentivirus	8 kb (ssRNA)	9 kb	Dividing and non-dividing cells	Stable
Adeno-associated virus	8.5 kb (ssRNA)	5 kb	Dividing and non-dividing cells	Stable and site-specific integration
Baculovirus	80-180 kb (dsDNA)	No upper limit known	Dividing and non-dividing cells	Transient or stable
Vaccinia virus	190 kb (dsDNA)	25 kb	Dividing cells	Transient
Herpes simplex virus	150 kb (dsDNA)	30-40 kb	Dividing and non-dividing cells	Transient

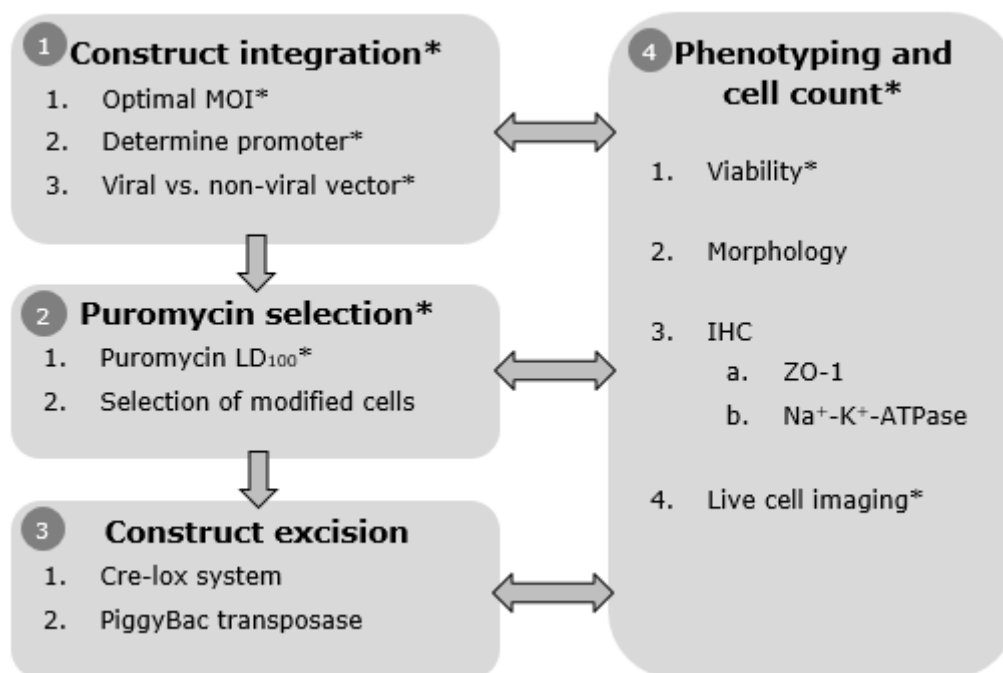



Figure A1: Schematic overview of the project involving the reversible immortalisation of primary HCEncs. The work packages and intermediate goals involving this master's thesis are indicated with an asterisk (*). The main goals of work package one are to find the optimal MOI, determine the best promoter and compare the construct integration between viral vs. non-viral vectors. In work package two, it will be tried to find the minimal lethal dose at which all cells die. This will be used to perform a selection of the modified cells. Work package three will be done to compare the excision efficiency between the Cre-lox system and the PiggyBac Excision-Only transposase. Finally, work package four contains different assays to determine cell phenotype in combination with cell counting which will be done in addition to the previous work packages. IHC, immunohistochemical

Table A2: Supplementary data of the HCEC-B4G12 cell line [89].

HCEC-B4G12	 Leibniz Institute DSMZ-German Collection of Microorganisms and Cell Cultures GmbH
ACC d47	
Cell line: HCEC-B4G12	
DSMZ no.: ACC 647	
Species: Human (<i>Homo sapiens</i>)	
Cell type: Corneal endothelium	
Origin: HCEC-B4G12 is a clonal subpopulation started in 2005 from the parental cell line HCEC-12 (ACC 646) established from normal cells of the posterior epithelium of the cornea of a 91-year-old Caucasian woman transformed with the early region of the SV40 genome including genes encoding large T-antigen and small t-antigen; the subclone is described in the literature to represent differentiated cells of the so-called corneal endothelium.	
Biosafety level: 1, GMO-S1	
DSMZ Cell Culture Data:	
Morphology: Cuboid epitheloid cells growing strongly adherent in monolayers	
Medium: Human-Endothelial-SFM + 10 ng/ml FGF-2 (observe the shelf-life of the medium; do not apply h.i. FBS in order to keep differentiation status)	
Subculture: Seed out at ca. 1×10^6 cells/80 cm ² flask: flasks must be coated with 10 µg/ml laminin and 10 mg/ml chondroitin sulfate: split confluent culture ca. 1:3 every 3-4 days using 2-3 ml trypsin/EDTA per 80 cm ² flask for 2-5 min at 37 °C (wash cells twice with PBS before trypsination, avoid trypsination longer than 5 min and check cell dissociation by microscopy): stop trypsination by using medium containing protease inhibitor cocktail (Sigma P1860) at 500-fold dilution; do not apply antibiotics, cells are highly sensitive to antibiotics	
Incubation: At 37 °C with 5% CO ₂	
Doubling time: Ca. 40-50 hours	
Harvest: Cell harvest of ca. 15×10^6 cells/175 cm ²	
Storage: Frozen with 90% medium (including FGF-2), 10% DMSO	
DSMZ Scientific Data:	
Mycoplasma: Negative in microbiological culture, PCR assays	
Immunology: To inquire about expression of EpCAM and intermediate filaments, contact hilmar.quentmeier@dsmz.de.	
Fingerprint: Fluorescent nonaplex PCR of short tandem repeat markers revealed a unique DNA profile (subclone of the cell line HCEC-12)	
Viruses: PCR: EBV -, HBV -, HCV -, HIV-1 -, HIV-2 -, HTLV-I/II -, MLV -, SMRV -	

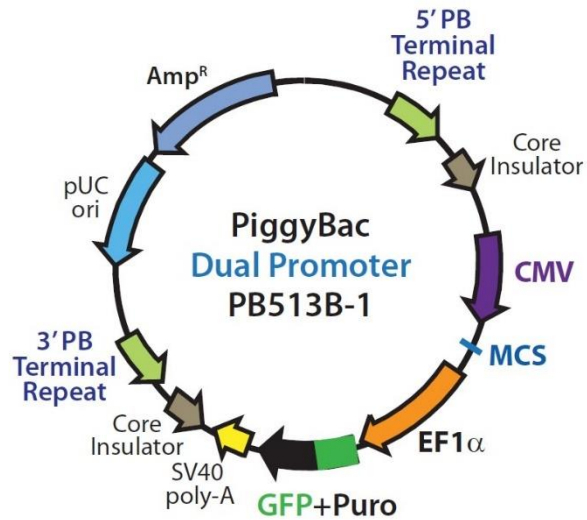


Figure A2: Plasmid map of the PiggyBac vector [91].

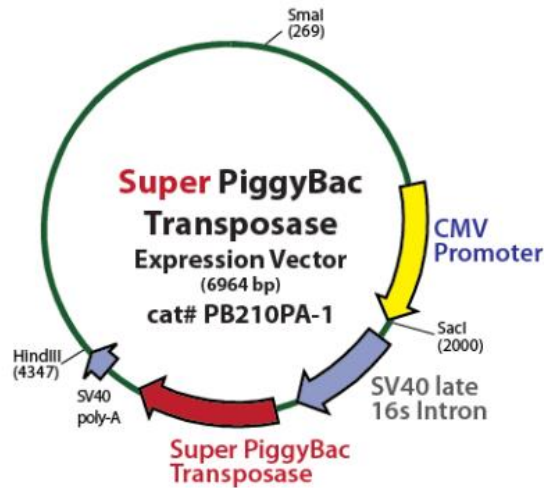


Figure A3: Plasmid map of the Super PiggyBac Transposase Expression Vector [91].

Table A3: All significant differences between the transduced cell yield of the different promoters after 4-hours of viral exposure at their specific MOI. Statistical testing was done by using the Kruskal-Wallis test followed by a post-hoc Dunn's multiple comparison test ($n=3$). CypA, cyclophilin A; CBA, chimeric cytomegalovirus-chicken B-actin; SFFV, spleen focus-forming virus

Promoters	MOI	Adjusted p-value
CypA vs. SFFV	0	0.0125
CypA vs. SFFV	0.1	0.0279
CypA vs. SFFV	0.3	0.0134
CypA vs. SFFV	1	0.0395
CypA vs. CBA	3	0.0279
CypA vs. CBA	5	0.0134

Table A4: All significant differences between the transduced cell yield of the different promoters after 24-hours of viral exposure at their specific MOI. Statistical testing was done by using the Kruskal-Wallis test followed by a post-hoc Dunn's multiple comparison test (n=3). CypA, cyclophilin A; CBA, chimeric cytomegalovirus-chicken B-actin; EF1a, elongating factor-1a; SFFV, spleen focus-forming virus

Promoters	MOI	Adjusted p-value
CypA vs. SFFV	0.1	0.0134
CBA vs. EF1a	0.5	0.0194
CBA vs. EF1a	1	0.0194
CypA vs. EF1a	3	0.0194
CypA vs. SFFV	10	0.0279
CypA vs. SFFV	30	0.0219

Table A5: Statistical analysis of the percentage of eGFP positive cells between 4- and 24-hours of viral exposure for each promoter. Statistical testing was done by using multiple t tests (n=3). CypA, cyclophilin A; CBA, chimeric cytomegalovirus-chicken B-actin; EF1a, elongating factor-1a; SFFV, spleen focus-forming virus

MOI	Adjusted p-value (4-hour vs. 24-hour viral exposure)			
	CypA	CBA	EF1A	SFFV
0	p>0.05	p>0.05	p>0.05	p>0.05
0.1	p>0.05	p>0.05	p>0.05	p>0.05
0.3	0.0241	0.0034	p>0.05	0.0495
0.5	0.0031	0.0054	p>0.05	0.0489
1	0.0044	0.0045	p>0.05	0.0215
3	0.0011	0.0001	0.0178	0.0221
5	0.0008	0.0003	0.0071	0.0025
10	0.0003	0.0003	0.0174	0.0489
15	NA	NA	p>0.05	NA
30	p>0.05	0.0001	NA	p>0.05

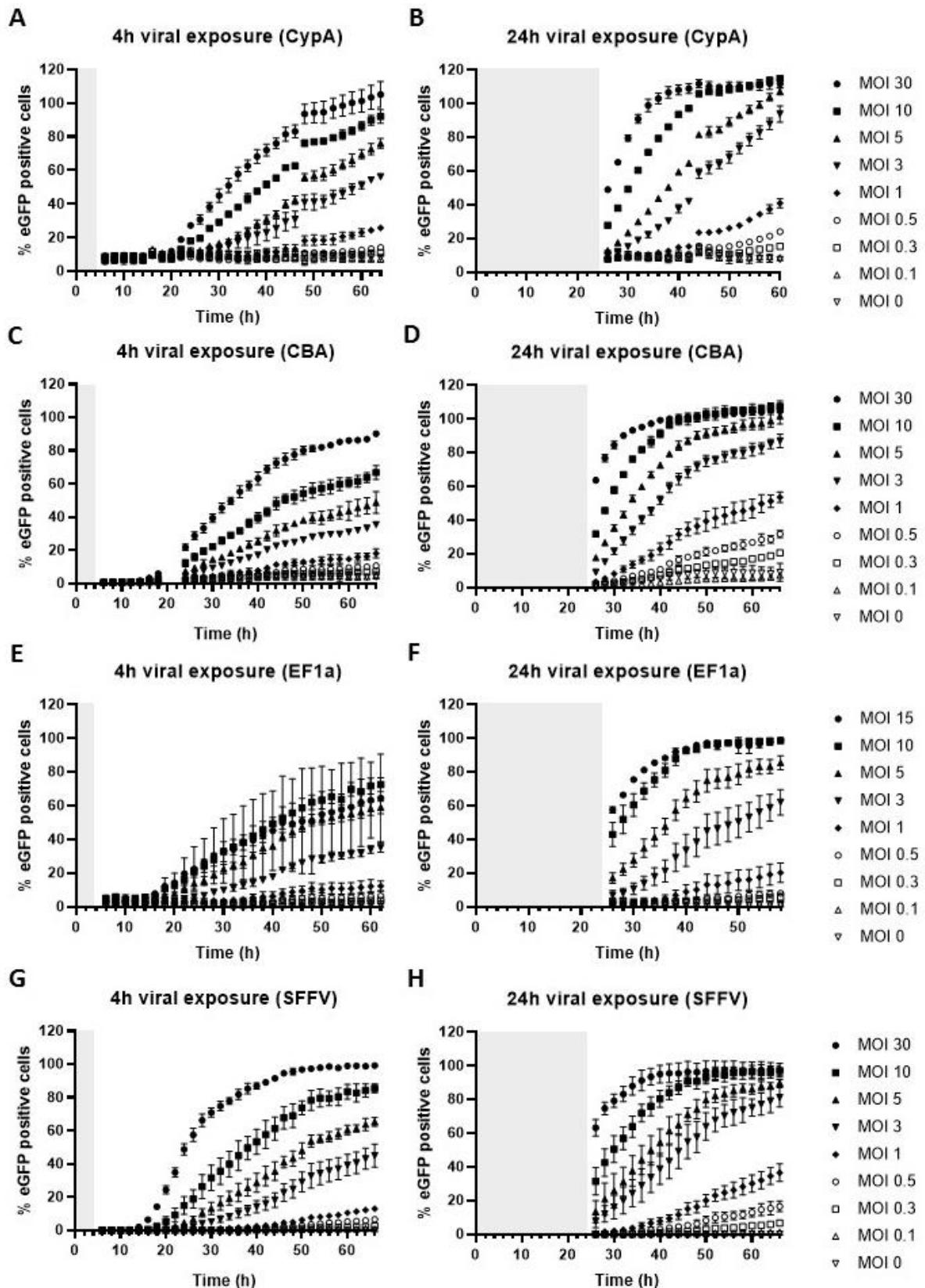


Figure A4: Percentage of eGFP positive cells in function of time after removal of viral vectors. For each vector different MOI were assessed for both 4-hour (A, C, E and G) and 24-hour viral exposure (B, D, F and H). Due to an unexpected maintenance of the IncuCyte a few data points are missing from the 4-hour CBA exposure graph (C) and because the vector containing the EF1a promoter had a relatively low titre, the highest MOI that could be reached was 15 instead of 30 ($n=3$). The grey box represents the incubation time during which no measurements could be taken due to interference with the viral vector. eGFP, enhanced green fluorescent protein; CypA, cyclophilin A; CBA, chimeric cytomegalovirus-chicken B-actin; EF1a, elongating factor-1a; SFFV, spleen focus-forming virus

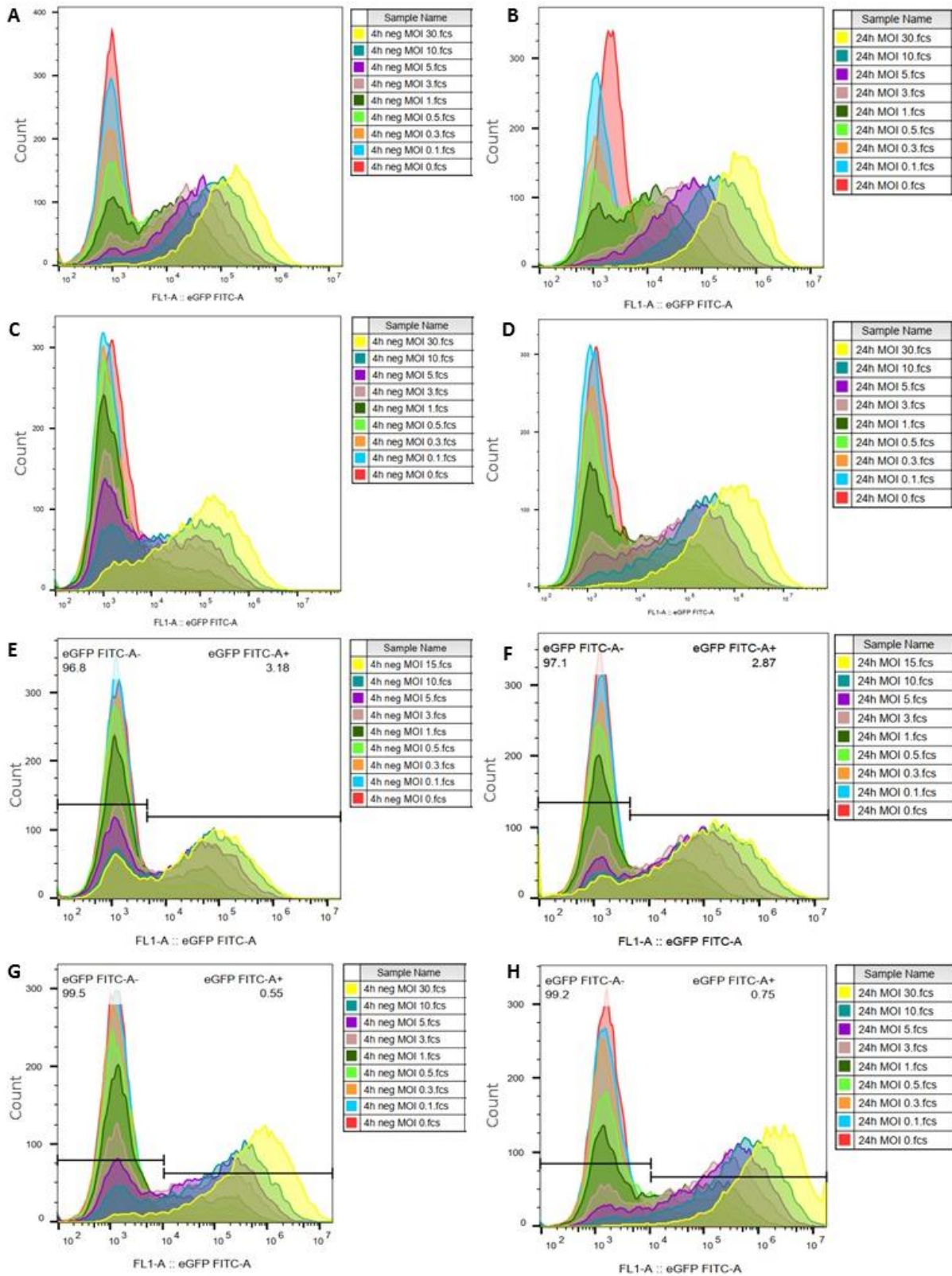


Figure A5: Representation of the flow cytometric data depicting count as a function of eGFP intensity after 4-hours of viral exposure for (A) CypA, (C) CBA, (E) EF1a and (G) SFFV and after 24-hours of viral exposure for (B) CypA, (D) CBA, (F) EF1a and (H) SFFV. eGFP, enhanced green fluorescent protein; CypA, cyclophilin A; CBA, chimeric cytomegalovirus-chicken B-actin; EF1a, elongating factor-1a; SFFV, spleen focus-forming virus

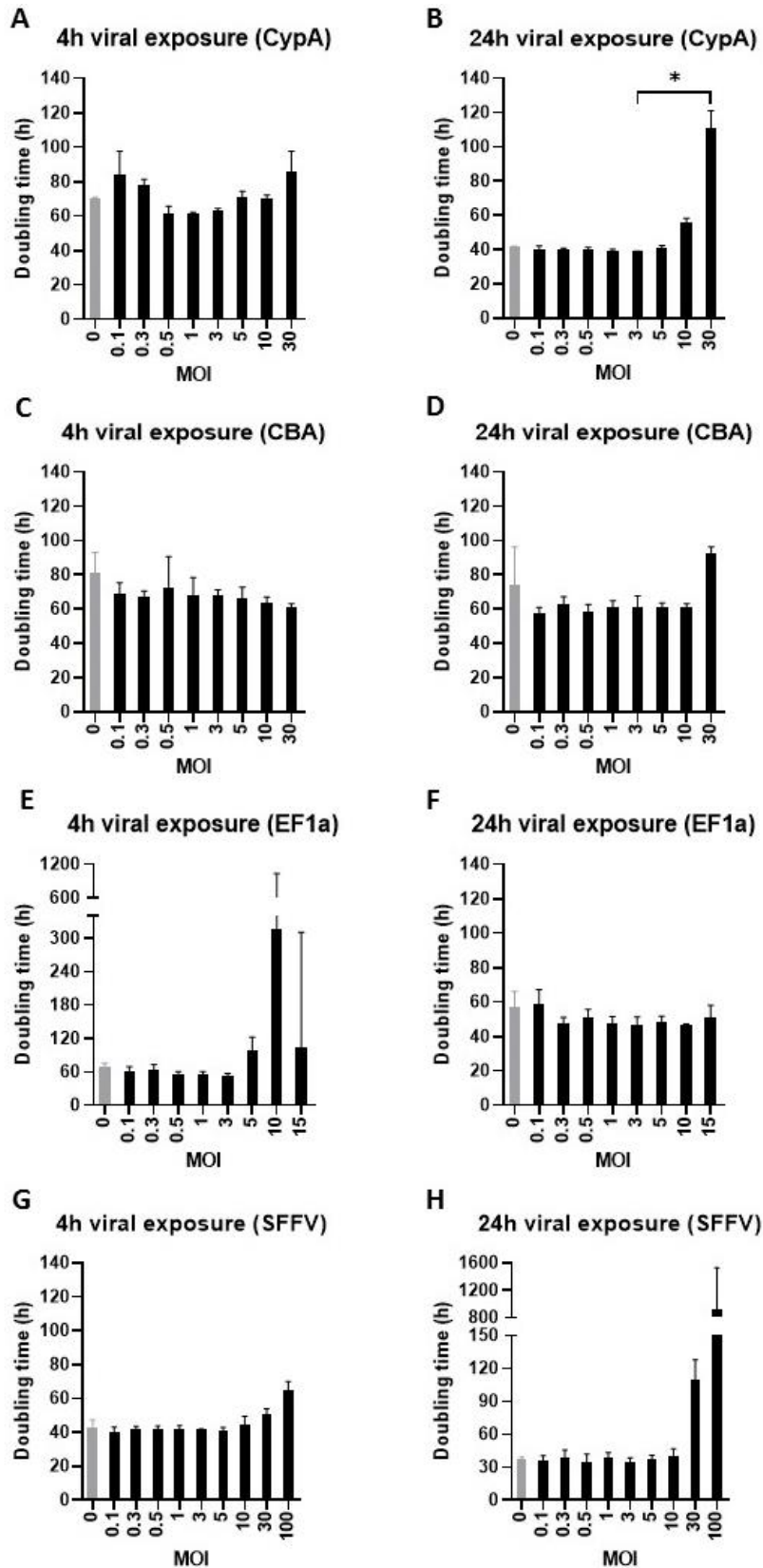


Figure A6: Population doubling time for all promoters for both the 4- and 24-hour viral exposure experiment. Using a Kruskal-Wallis test followed by Dunn's multiple comparison test, a significant difference was found between MOI 3 and 30 in the 24-hour CypA experiment ($p = 0.0298$; $n=3$). eGFP, enhanced green fluorescent protein; CypA, cyclophilin A; CBA, chimeric cytomegalovirus-chicken B-actin; EF1a, elongating factor-1a; SFFV, spleen focus-forming virus

Table A6: All significant differences between the cell doubling times of the different promoter after 4-hours of viral exposure at their specific MOI. Statistical testing was done by using the Kruskal-Wallis test followed by a post-hoc Dunn's multiple comparison test (n=3). CypA, cyclophilin A; CBA, chimeric cytomegalovirus-chicken B-actin; EF1a, elongating factor-1a; SFFV, spleen focus-forming virus

Promoters	MOI	Adjusted p-value
SFFV vs. CBA	0	0.0194
SFFV vs. CypA	0.1	0.0194
SFFV vs. CypA	0.3	0.0134
SFFV vs. CBA	0.5	0.0279
SFFV vs. CBA	3	0.0134
SFFV vs. EF1a	5	0.0134
SFFV vs. CypA	30	0.0219

Table A7: All significant differences between the cell doubling times of the different promoters after 24-hours of viral exposure at their specific MOI. Statistical testing was done by using the Kruskal-Wallis test followed by a post-hoc Dunn's multiple comparison test (n=3). CypA, cyclophilin A; CBA, chimeric cytomegalovirus-chicken B-actin; SFFV, spleen focus-forming virus

Promoters	MOI	Adjusted p-value
SFFV vs. CBA	0	0.0297
CypA vs. CBA	0.3	0.0395
SFFV vs. CBA	0.5	0.0395
SFFV vs. CBA	1	0.0395
SFFV vs. CBA	3	0.0134
SFFV vs. CBA	5	0.0194
SFFV vs. CBA	30	0.0132

Table A8: Statistical analysis of the cell doubling time between 4- and 24-hours of viral exposure for each promoter. Statistical testing was done by using multiple t tests (n=3). CypA, cyclophilin A; CBA, chimeric cytomegalovirus-chicken B-actin; EF1a, elongating factor-1a; SFFV, spleen focus-forming virus

MOI	Adjusted p-value (4-hour vs. 24-hour viral exposure)			
	CypA	CBA	EF1A	SFFV
0	0.00002	p>0.05	p>0.05	p>0.05
0.1	0.0104	p>0.05	p>0.05	p>0.05
0.3	0.0003	p>0.05	p>0.05	p>0.05
0.5	0.0063	p>0.05	p>0.05	p>0.05
1	0.00003	p>0.05	p>0.05	p>0.05
3	0.00002	p>0.05	p>0.05	p>0.05
5	0.0005	p>0.05	p>0.05	p>0.05
10	0.0063	p>0.05	p>0.05	p>0.05
15	NA	NA	p>0.05	NA
30	p>0.05	0.0024	NA	0.0408

